JCI The Journal of Clinical Investigation

Hijacking a key chromatin modulator creates epigenetic vulnerability for Myc-driven cancer

Zhenhua Yang, … , Wei Li, Hao Jiang

J Clin Invest. 2018. https://doi.org/10.1172/JCI97072.

Research Article In-Press Preview Hematology Oncology

Graphical abstract

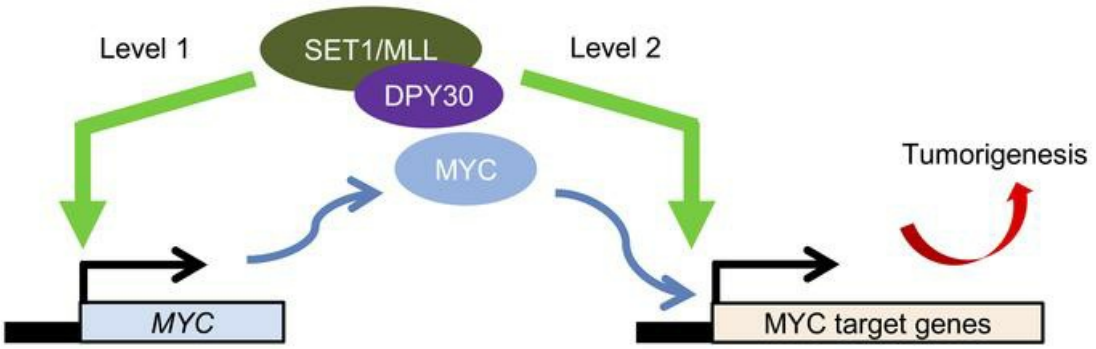

Hijacking a key chromatin modulator creates epigenetic vulnerability for MYC-driven cancer

***Zhenhua Yang[1], *Kushani Shah[1], Theodore Busby[1], Keith Giles[1], Alireza Khodadadi-Jamayran[1], Wei Li[1,2], and Hao Jiang[1, 2]§**

[1]Department of Biochemistry and Molecular Genetics, UAB Stem Cell Institute, University of Alabama at Birmingham School of Medicine
[2]Department of Biochemistry and Molecular Genetics, University of Virginia School of Medicine

* These authors contributed equally to this work

§Corresponding author:

Hao Jiang
Department of Biochemistry and Molecular Genetics
University of Virginia School of Medicine
PO Box 800733
1340 JPA, Pinn Hall Room 6017
Charlottesville, VA 22908
Phone: (434) 924-2112
Email: hj8d@virginia.edu

The authors have declared that no conflict of interest exists.

ABSTRACT

While the genomic binding of MYC protein correlates with active epigenetic marks on chromatin, it remains largely unclear how major epigenetic mechanisms functionally impact the tumorigenic potential of MYC. Here we showed that compared to the catalytic subunits, the core subunits, including DPY30, of the major H3K4 methyltransferase complexes were frequently amplified in human cancers, and selectively upregulated in Burkitt lymphoma. We showed that DPY30 promoted expression of endogenous *MYC*, and was also functionally important for efficient binding of MYC to its genomic targets by regulating chromatin accessibility. *Dpy30* heterozygosity did not affect normal animal physiology including life span, but significantly suppressed Myc-driven lymphomagenesis, as cells failed to combat oncogene-triggered apoptosis due to insufficient epigenetic modulation and expression of a subset of anti-apoptotic genes. Dpy30 reduction also greatly impeded MYC-dependent cellular transformation without affecting normal cell growth. These results suggest that MYC hijacks a major epigenetic pathway -- H3K4 methylation -- to facilitate its molecular activity in target binding and to coordinate its oncogenic program for efficient tumorigenesis, meanwhile creating “epigenetic vulnerability”. DPY30 and the H3K4 methylation pathway are thus potential epigenetic targets for treating certain MYC-driven cancers.

INTRODUCTION

C-MYC (hereafter MYC) is an important oncogene that is hyper-activated and a central driving force in a wide spectrum of human cancers (1). MYC can be activated through gene amplification or translocation, the latter probably best exemplified by human Burkitt lymphoma (BL) featuring *MYC*/*Immunoglobulin* (*Ig*) chromosomal translocations (2, 3). The *Eμ-Myc* transgenic mice develop aggressive B cell lymphomas as a result of the *Myc* transgene activation under the control of *Ig Eμ* enhancer (4), and have been a highly valuable model for studies of human BL and for understanding mechanisms regulating MYC-driven tumorigenesis (5, 6).

MYC drives tumorigenesis mainly by acting as a transcription factor that binds to numerous genomic sites and regulates the expression of a large number of target genes (7). While MYC has been proposed to be a universal amplifier of all activated genes in the genome (8, 9), it is also argued that the selective regulation of different target transcription by MYC underlies MYCs role in tumorigenesis (7, 10, 11). In either model, efficient binding of MYC to its genomic targets is invariably crucial to its oncogenic activity. While it has been long known that MYC recognizes the E-box element in the genome, a better correlation was shown between MYC binding sites and epigenetic marks associated with active transcription in the genome, such as histone H3 K4/K79 methylation and H3 acetylation (12, 13). However, outstanding questions remain regarding (i) the causal relationship between MYC binding and occupancy of the epigenetic marks, (ii) whether MYC and the relevant epigenetic modulators regulate each other, and (iii) what the functional impact and significance of such regulation might be.

Histone H3K4 methylation not only is one of the most prominent epigenetic marks associated with active or poised transcription (14), but also functionally regulates chromatin transcription (15, 16). As the major H3K4 methylation enzymes in mammals, the SET1/MLL complexes comprise of SET1A or 1B, or MLL1, 2, 3, or 4 as the catalytic subunit, and WDR5, RbBP5, ASH2L, and DPY30 as integral common core subunits necessary for the full methylation activity (Diagram in Figure 1A) (17). Human *MLL1* is a common target of chromosomal translocations in acute leukemias, and genetic lesions and/or altered expression of other subunits are extensively associated with a variety of human cancers (18-26). Compared to the large number of correlative studies, functional evidence of these subunits in tumorigenesis is rather limited, and the role of the H3K4 methylation activity in tumorigenesis remains elusive.

We have previously established a direct role of DPY30 in facilitating genome-wide H3K4 methylation, especially H3K4 tri-methylation (H3K4me3) (27), which allows us to investigate the functional roles of efficient H3K4 methylation in physiological and pathological processes by genetically manipulating DPY30. Further studies by us and others have identified important roles of DPY30 in regulating fundamental cellular processes including cell growth (28, 29), differentiation (27, 28), and senescence (29), and stem cell fate determination (27, 30, 31). While we have previously shown that DPY30 directly regulates the expression of the endogenous *MYC* gene and is important for the growth of several MLL-rearranged leukemia cell lines in culture (28), a role of DPY30 in cancer has not been further demonstrated. In this work, we set out to address a functional role of DPY30 in regulating the molecular activity of MYC in tumorigenesis.

RESULTS

SET1/MLL complex core subunits including DPY30 are upregulated in Burkitt lymphoma

To systematically examine the roles of the different SET1/MLL complex subunits in human cancers, we started by analyzing their genetic alterations using the cBio Cancer Genomics Portal (32). Surprisingly, our analyses reveal that while most of the catalytic subunits are frequently mutated, the core subunits are often amplified, across a wide variety of human cancers (Supplemental Figure 1). Such alterations suggest tumor-suppressing roles of the catalytic subunits, but possibly tumor-promoting roles of the core subunits of the SET1/MLL complexes.

As differential functions often require differential regulation, we sought regulatory mechanisms of these subunits related to oncogenesis. We have previously shown that high level of Myc directly promotes the expression of several subunits of the Set1/Mll complexes, especially Wdr5 and Dpy30, in mouse embryonic fibroblast (MEFs) (30). To assess the impact of MYC on the expression of these methylation modulators in a more clinically relevant setting, we queried expression data sets of primary human BL samples with *MYC/Ig* translocations versus non-BL subtypes (33). We found that the expression of the core (including DPY30, ASH2L, and RbBP5), but not most catalytic subunits of SET1/MLL complexes, is significantly upregulated in BL samples versus non-BL subtypes (Figure 1A). Using data sets from the *Eμ-Myc* lymphomagenesis mouse model (10), we again found that the expression of the core, but not the catalytic subunits is upregulated in the *Eμ-Myc* pre-tumor B cells compared to the control B cells (Figure 1B, Supplemental Figure 2). Moreover, Myc binds to genes encoding the core, but not most catalytic subunits in *Eμ-Myc* pre-tumor B cells and lymphomas (Figure 1C, Supplemental Figure 2). These results indicate that the expression of core subunits of the SET1/MLL complexes are directly and selectively promoted by MYC, suggesting their potential role in MYC's function in tumorigenesis. Such differential regulation befits the divergent alterations of these subunits in human cancer.

Further analyses of a wide variety of cancer types in cBio Cancer Genomics Portal show that nearly 50% of studies (among studies with sufficient sample numbers with available data) find notable elevation of *DPY30* expression in tumors with increased copy number of at least one of the three *MYC* genes (*C-MYC*, *N-MYC*, and *L-MYC*, Supplemental Figure 3A). Therefore, the association between *MYC* and *DPY30* overexpression is not tumor type specific. This is consistent with our conclusion that MYC binds to *DPY30* gene and directly promotes its expression. *DPY30* overexpression and *MYC* amplification/overexpression do not necessarily overlap in patient tumor samples (Supplemental Figure 3B), suggesting a complex regulation of *DPY30* expression by *MYC* and other mechanisms in vivo.

DPY30 regulates expression of *MYC* and MYC target genes

To study a functional role of the SET1/MLL complex core subunits in MYC-driven tumorigenesis, we started with Raji, a BL cell line, and Jurkat, an acute T lymphoblastic leukemia cell line that expresses (34) and is dependent (35) on high level of MYC. We found that the growth of both cells was significantly inhibited by DPY30 knockdown (KD) (Supplemental Figure 4A). Moreover, expression of *MYC* and *MAX*, which encodes an important partner of MYC (36), was significantly reduced upon DPY30 KD (Supplemental Figure 4B, C). This is consistent with our previous findings that DPY30 directly regulates the endogenous *MYC* expression in human *MLL1*-rearranged leukemia cells (28).

To facilitate further functional studies, we used P493-6 cells, a human BL cell model that express a tetracycline-repressible *MYC* transgene, but negligible level of endogenous *MYC* (37). We found that, similar to turning off MYC (Figure 2A), DPY30 or WDR5 KD also abolished their growth (Figure 2B). DPY30 KD greatly reduced proliferation of P493-6 cells with little effect on apoptosis (Supplemental Figure 5A-D). Consistent with these cellular phenotypes, our microarray results (Supplemental Figure 5E) showed that DPY30 KD in P493-6 cells downregulated a subset of genes involved in cell cycle

progression, such as *CCNA2, CCND2, MCM10, CDCA7, CDCA5*, but not most of other pro-survival genes (except for *BIRC5*).

Further analysis of the microarray results (Figure 2C, Supplemental Table 1) revealed a correlation between the effects of DPY30 KD and MYC silencing on gene expression. Most genes that were markedly downregulated by DPY30 KD were also downregulated by MYC silencing (Figure 2C), supporting a co-regulation of a large subset of genes by DPY30 and MYC. We next assessed the impact of DPY30 loss on MYC-mediated global gene reprogramming. We turned off *MYC* expression by tetracycline and then turned it back on by washing tetracycline away (Figure 2D). While turning MYC off downregulated expression of *WDR5* and *DPY30*, turning MYC back on restored their expression (Figure 2D), further demonstrating the regulation of their expression by MYC. We did such treatment to both control and DPY30-KD P493-6 cells and examined global gene expression change after 4 hours of MYC reactivation, reasoning that such short period of MYC reactivation mainly affects direct targets of MYC. We found that DPY30 KD significantly dampened the upregulation of most MYC-induced genes, and also significantly impaired the downregulation of most MYC-repressed genes (Figure 2E, Supplemental Table 1). In other words, DPY30 loss blunts the transcription reprogramming mediated by MYC reactivation. Taken together, our results indicate that DPY30 functionally regulates the expression of MYC targets.

Dpy30 is important for efficient binding of Myc to its genomic loci

Unlike the regulation of the endogenous *MYC* by DPY30 (Supplemental Figure 4B) (28, 31), expression of the tetracycline-controlled *MYC* transgene was not affected by DPY0 KD at either RNA or protein level in P493-6 cells (Figure 3A, B). Moreover, expression of *MAX* was also not affected (Figure 3A). How then were MYC targets dysregulated following DPY30 KD?

We next assessed if binding of MYC to its genomic targets was affected by DPY30 KD by performing MYC ChIP assays followed by both sequencing and qPCR assays. We first confirmed the specificity of our Myc antibody for ChIP by showing that MYC ChIP signals were dramatically reduced at all examined MYC targets after silencing MYC (Supplemental Figure 6A). Binding of MYC upon DPY30 KD was markedly reduced at a subset of gene transcription start sites (TSSs) and modestly reduced at the majority of TSSs (Figure 3C, Supplemental Table 2). While a small subset of genes showed increase in MYC binding, they do not appear to be major MYC targets due to the very low MYC signals at their TSSs (Figure 3C, Supplemental Figure 6B). We also performed H3K4me3 ChIP assays. Consistent with previous findings (12, 13), there is a general correlation between MYC binding and H3K4me3 throughout the genome (Supplemental Figure 6C). H3K4me3 was appreciably reduced at TSSs that showed reduced MYC binding upon DPY30 KD, but not at those that showed increased MYC binding (Figure 3C, D, Supplemental Figure 6D, Supplemental Table 3). We note that because the counts of reads in any specific regions were normalized to total counts of reads in the sample, the reduction seen on local MYC or H3K4me3 was most likely underestimated throughout the genome. Nevertheless, the relative effects for different gene loci are preserved. Our ChIP-qPCR assays confirmed a consistent decrease of MYC binding and H3K4me3 in several representative MYC target genes in all gene subsets, although the extent of decrease somewhat differs among different subsets (Figure 3E and Supplemental Figure 7). We also examined the proliferation or survival-associated genes that were downregulated by DPY30 KD in P493-6 cells, and found that *CCND2, CDCA7*, *CDCA5*, and *BIRC5* were bound by MYC, and both MYC binding and H3K4me3 at these genes were reduced upon DPY30 KD (Supplemental Figure 5F). Moreover, Dpy30 KD in MEFs (Supplemental Figure 6E) also markedly reduced Myc binding to a few established Myc targets (Supplemental Figure 6F), indicating that the effect of Dpy30 depletion on genomic binding of Myc is not limited to P493-6 cells.

We also studied the role of the ASH2L subunit, which directly binds to DPY30 and links it to the SET1/MLL complexes to facilitate H3K4 methylation (38). ASH2L is also amplified in many cancers (Supplemental Figure 1) and directly upregulated by activated MYC (Figure 1). Similar to DPY30 KD, ASH2L KD also

abolished the growth of P493-6 cells (Supplemental Figure 8A), with little effect on tetracycline-controlled *MYC* expression (Supplemental Figure 8B). H3K4me3 was markedly reduced at almost all loci that we previously examined for DPY30 KD, and MYC binding was appreciably reduced at many of these loci (Supplemental Figure 8C). These results further support a role of the H3K4 methylation pathway in regulating MYC binding to its genomic targets.

To further understand how DPY30 and ASH2L regulate the genomic binding of MYC, we examined their physical interaction in in vitro binding assays. Consistent with previous reports (39), ASH2L directly binds to MYC. However, DPY30 failed to show a direct binding with MYC (Supplemental Figure 9A). Therefore, DPY30 does not affect MYC's activity through directly binding to MYC. As shown by ATAC (40) and DNase I hypersensitivity assays, chromatin accessibility was reduced at assessed loci upon the reduction of Dpy30 and global H3K4me3 levels (Figure 4A-D, Supplemental Figure 9B). Taken together, our results suggest that Dpy30-regulated chromatin setting functionally influences Myc's activity in transcription, prompting us to study a role of Dpy30 in Myc-driven tumorigenesis in vivo.

Full level of Dpy30 is not required for normal animal development, physiology, and life span

As Dpy30 loss in the hematopoietic system results in pancytopenia (31), we first examined the effect of genetically reducing Dpy30 dose on normal animal physiology. Compared to $Dpy30^{F/+}$ littermates ("*F*" is the conditional allele) (31), $Dpy30^{F/-}$ mouse embryos (Figure 5A) reduced *Dpy30* expression about 50% at RNA (Figure 5B) and protein (Figure 5C) levels, had slightly (and insignificantly) reduced global H3K4me3 level in their fetal livers cells (Figure 5C), and were indistinguishable in the gross morphology (Figure 5D). Compared to the wild type (WT) littermates, splenic B cells from $Dpy30^{+/-}$ mice also reduced *Dpy30* expression about 50% at RNA (Figure 7B) and modestly at protein (Figure 5E) levels, and had modestly reduced global H3K4me3 level (Figure 5E). Young developing $Dpy30^{+/-}$ mice had slightly albeit significantly lower body weight than their WT littermates for both sexes (Figure 5F), but appeared completely healthy with a normal peripheral blood profile (Figure 5G). Importantly, after following up these animals for 3 years, we found that the $Dpy30^{+/-}$ mice had the same life span as the WT littermates (Figure 5H). Moreover, *Dpy30* heterozygosity did not significantly affect the spleen weight or the development, size, proliferation, and apoptosis of the spleen and bone marrow B cells (Figure 6B-F, Supplemental Figure 10A). No significant alteration of cellular damage signals such as DNA damage response (Supplemental Figure 10B) or reactive oxygen species (ROS) level (Supplemental Figure 10C) was detected following inactivation of one *Dpy30* allele. Therefore, we conclude that the full level of Dpy30 is largely dispensable for normal animal physiology.

***Dpy30* heterozygosity suppresses Myc-driven lymphomagenesis**

We then studied effects of Dpy30 reduction in the *Eμ-Myc* lymphomagenesis mouse model. We found that *Eμ-Myc;* $Dpy30^{+/-}$ mice survived significantly longer than their *Eμ-Myc* littermates with a near 50% increase in the median survival time (Figure 6A), and significantly mitigated Myc-driven spleen enlargement (Figure 6B). These results demonstrate that reducing Dpy30 level suppresses Myc-driven lymphomagenesis without affecting normal physiology.

We found that *Dpy30* heterozygosity modestly but significantly mitigated the developmental block from pre-B to mature B cells and the cell size increase caused by the *Eμ-Myc* transgene (Figure 6C, D, Supplemental Figure 10A). *Eμ-Myc* activation dramatically increased proliferation of all B cells in spleen and bone marrow. We found that *Dpy30* heterozygosity modestly but significantly reduced proliferation of certain subpopulations of B cells in spleen (Figure 6E). All these results are consistent with a reduced Myc activity in B cells upon inactivation of one *Dpy30* allele.

We then examined B cell apoptosis. Although Myc hyperactivation can elicit apoptosis of human fibroblasts (41), no significant increase in apoptosis of splenic or bone marrow B cells was detected in

Eμ-Myc mice with intact Dpy30 level except the $B200^{+}IgM^{+}IgD^{-}$ subpopulation in bone marrow (Figure 6F). When one *Dpy30* allele was inactivated, however, apoptosis was significantly and markedly increased for *Eμ-Myc* B cells at all developmental stages in spleen, and for the overall B cell populations in bone marrow (Figure 6F). Therefore, cellular stresses imposed by *Myc* hyperactivation would have elicited strong apoptosis had it not been for sufficient level of Dpy30 and its enforced elevation by Myc (further shown and discussed later).

Since Dpy30 depletion in human fibroblasts results in increase in DNA damage response and ROS (29), we examined if these also occur in *Dpy30* heterozygous B cells. We found that while the total level of phosphorylated H2AX (γ-H2AX) and ROS were markedly increased in the splenic B cells of *Eμ-Myc* compared to WT mice, *Dpy30* heterozygosity did not affect the levels of these signals or total p53 (Supplemental Figure 10B, C). Therefore, *Dpy30* heterozygosity does not induce apoptosis by increased DNA damage or ROS.

Effect of *Dpy30* heterozygosity on gene expression in B cells at different malignant stages

We next determined the impact of *Dpy30* heterozygosity on gene expression in B lymphocytes in the absence and presence of the *Eμ-Myc* transgene, using $B200^{+}$ splenocytes from non-transgenic control mice and premalignant *Eμ-Myc* mice. Total RNA amount per cell was dramatically increased by *Eμ-Myc* expression, but was not affected by *Dpy30* heterozygosity in B cells regardless of the transgene (Figure 7A). *Dpy30* expression was upregulated over 2 fold by *Eμ-Myc*, reduced to half by inactivation of one *Dpy30* allele either in the absence or presence of the *Eμ-Myc*, and was similar between WT and *Eμ-Myc; Dpy30*$^{+/-}$ B cells (Figure 7B). Expression of *Myc* or *Max* was not significantly affected by *Dpy30* heterozygosity (Figure 7B, C). Global H3K4me3 level was modestly reduced in *Eμ-Myc; Dpy30*$^{+/-}$ compared to *Eμ-Myc* B cells (Figure 7C). Using spike-in RNA control, our RNA-seq analyses followed by Gene Set Enrichment Analysis (GSEA) (42) showed that the genes downregulated in *Eμ-Myc; Dpy30*$^{+/-}$ compared to *Eμ-Myc* B cells were significantly enriched with genes bound and activated by Myc (Figure 7D left, Supplemental Figure 11 and Supplemental Table 4, 5), and that the upregulated genes were enriched with genes bound and repressed by Myc (Figure 7D right, Supplemental Figure 11 and Supplemental Table 4, 5). Moreover, our gene ontology analyses revealed that genes downregulated by *Dpy30* heterozygosity in the presence of *Eμ-Myc* were enriched with common Myc targets such as genes in ribosome and RNA biogenesis (Supplemental Figure 12A, Supplemental Table 6). These results in animals are consistent with those in P493-6 cells, in which the expression of Myc targets, but not *Myc* itself, is dysregulated upon Dpy30 loss.

Consistent with the increased apoptosis, expression of cytotoxic genes such as *FasL* and *Gzmb* was significantly upregulated (Supplemental Figure 12B, Supplemental Table 6), while a subset pro-survival genes such as *Mt1* (43, 44) and *Bcl-xL* (45) was significantly downregulated in the *Eμ-Myc; Dpy30*$^{+/-}$ compared to *Eμ-Myc* B cells (Figure 7E). We found that Dpy30 bound to the TSSs of *Mt1*, *Birc5* and *Bcl-xL* genes in splenic B cells (Figure 7F), suggesting a direct regulation of these pro-survival genes by Dpy30, although the extent of consequence on their expression varied upon Dpy30 reduction. A further dissection around the *Mt1* TSS region showed that, consistent with the induction of *Mt1* by *Eμ-Myc* (Figure 7E), Dpy30 was increasingly recruited to *Mt1* TSS following *Eμ-Myc* activation, resulting in enhanced H3K4 methylation (Supplemental Figure 13). Upon inactivation of one *Dpy30* allele in the presence of *Eμ-Myc* transgene, promoter binding of Dpy30 was reduced, leading to reduced H3K4me3 (Supplemental Figure 13) and inefficient expression of *Mt1*. These results suggest that Myc promotes Dpy30 to ensure sufficient expression of certain pro-survival genes to suppress otherwise detrimental apoptotic response to cancer cells.

To understand how lymphomas eventually formed in the *Eμ-Myc; Dpy30*$^{+/-}$ mice, we examined the expression of all subunits of Set1/Mll complexes and pro-survival genes in these tumor samples. *Dpy30* expression in *Eμ-Myc; Dpy30*$^{+/-}$ lymphomas was still reduced to ~50% at the RNA and markedly reduced

at the protein levels compared to the *Eμ-Myc* lymphomas (Supplemental Figure 14). Expression of all other catalytic and core subunits of the Set1/Mll complexes and Myc was not significantly altered (Supplemental Figure 14). While *Bcl-xl* expression was significantly reduced, *Mt1* expression was no longer affected by *Dpy30* heterozygosity in lymphomas (Supplemental Figure 14A). These results suggest that altered regulation of selected Dpy30 targets may allow bypass of the Dpy30 pathway and underlie the ultimate formation of tumors despite the reduction of Dpy30.

Dpy30 is haploinsufficient for cellular transformation, but not for normal growth

To determine if the differential requirement of Dpy30 dose is limited to *Eμ-Myc*-driven lymphomagenesis, we studied the impact of *Dpy30* heterozygosity on transformation of primary MEFs by two potent oncogenes, *H-RAS*^{G12V} and *MYC*. *Dpy30* heterozygosity reduced *Dpy30* mRNA level about 50% (Figure 8B), and did not significantly affect the growth of primary MEFs (Figure 8A). DPY30 expression was upregulated about 3 fold following H-RAS^{G12V} and MYC transduction of the WT MEFs (Figure 8B), but not after transduction of H-RAS^{G12V} alone (data not shown), further supporting its regulation by Myc. Again, Dpy30 level was reduced to about 50% in transduced *Dpy30*$^{+/-}$ MEFs, but was still higher than that in untransduced WT MEFs (Figure 8B). We also determined that expression levels of both oncogenes were comparable between the WT and *Dpy30*$^{+/-}$ MEFs (Figure 8B). As reflected by the anchorage-independent colony formation, the WT MEFs were efficiently transformed by these oncogenes. Transformation of *Dpy30*$^{+/-}$ MEFs, however, was dramatically impeded (Figure 8C and Supplemental Figure 15A). In vivo tumorigenicity of the transduced MEFs was also significantly reduced by *Dpy30* heterozygosity (Figure 8D). While proliferation was similar between WT and *Dpy30*$^{+/-}$ MEFs following RAS-MYC transduction, apoptosis (and general cell death) was significantly higher in the *Dpy30*$^{+/-}$ than the WT MEFs after transduction (Supplemental Figure 16), consistent with the observations in the *Eμ-Myc* B cells. These results reveal a contrasting requirement of Dpy30 dose – while the regular Dpy30 level is more than enough for normal cell growth, it must be elevated for efficient cancerous transformation by oncogenes, possibly through combating oncogene-associated apoptotic stress.

We next assessed the direct consequences of overexpression of the SET1/MLL complex core subunits in cellular transformation. A previous work (24) has shown that primary rat embryonic fibroblasts can be transformed by overexpressing RAS^{G12V} and ASH2L. Here we found that MEFs that overexpress RAS^{G12V} together with either DPY30 or ASH2L formed colonies in soft agar, although the number of colonies was less than that by RAS^{G12V} and MYC (Supplemental Figure 15B). Interestingly, while the combination of RAS^{G12V} with ASH2L or with DPY30 gave rise to similar number of total colonies, RAS^{G12V} with ASH2L did not give rise to large colonies like RAS^{G12V} with DPY30 or with MYC (Supplemental Figure 15B). These results indicate that DPY30 and ASH2L each individually can cooperate with RAS^{G12V} to promote transformation. The similar phenotype suggests they regulate a common pathway (presumably Set1/Mll complexes-mediated H3K4 methylation) in promoting transformation, but the difference in the colony size suggests that Dpy30 may regulate additional pathways in controlling transformation.

DISCUSSION

Our studies reveal a functional relationship between a major epigenetic mechanism and an important oncogene. We have previously shown that DPY30 directly regulates the expression of endogenous *MYC* in hematopoietic cells (28, 31). Here we reinforced this conclusion in other MYC-overexpressing blood cancer cells, and show that MYC also directly regulates the expression of several core subunits, including DPY30, of the major H3K4 methyltransferase complexes in several cellular systems. Therefore, DPY30 and MYC mutually and positively regulate each other. The direct upregulation of *DPY30* by MYC is functionally important, as insufficient DPY30 level clearly impairs MYC-driven lymphomagenesis and cellular transformation.

Although H3K4 methylation is well known to be intimately associated with active transcription and biochemically capable of directly enhancing chromatin transcription, its biological functions in physiology and pathology are surprisingly murky, partly due to the complex composition and functions of the many subunits of the complexes collectively responsible for the enzymatic activity. Most of the core subunits of SET1/MLL complexes are considered essential for the efficient H3K4 methylation activity of all six catalytic subunits (46), and their expression levels are thus generally expected to be limiting for gene expression in cells and physiology of animals. Our results here show that the Dpy30 subunit exists in excess for normal physiology from embryonic development to life span of the animal, raising the question of the purpose to keep this subunit in a surplus level. One possible explanation is its potential role in dealing with stressed conditions. In this work, we show that oncogenic activation such as MYC overexpression not only co-opts the existing excessive DPY30 level, but also directly and selectively upregulates its expression (and other SET1/MLL complex core subunits) to play a critical role in tumorigenesis. Such upregulation is necessary, because a Dpy30 level similar to or just modestly higher than that in normal cells (as seen in the Myc-overexpressing *Dpy30*$^{+/-}$ B cells and MEFs, Figure 7B and 8B) is insufficient for tumorigenesis. Therefore, the hyper-activated *MYC* oncogene, in a sense, has evolved to hijack key chromatin modulators to promote tumorigenesis.

The selective regulation of the core but not the catalytic subunits of the SET1/MLL complexes by MYC is consistent with the divergent alterations and possibly divergent roles of these subunits in human cancers. Indeed, mutations (mostly loss-of-function) in genes encoding the catalytic subunits of the SET1/MLL complexes are among the most frequent genetic lesions in human cancers (19-21, 23, 26, 47, 48). Moreover, the tumor suppressive role of some of these subunits have been demonstrated (49, 50). On the other hand, genetic mutations of the core subunits are rarely found in human cancers. Instead, the DPY30 (51), ASH2L (24, 52), and WDR5 (25, 53, 54) core subunits have been found to be overexpressed in cancers, show correlation of high expression levels with poor prognosis, and in some cases functionally promote tumorigenesis. Such differential regulations and roles elicit interesting questions worthy of further investigation relating to the exact roles of these subunits and the associated H3K4 methylation in cancer.

Our previous and current studies have collectively uncovered two different levels of regulation of MYC activity by DPY30 (Figure 8E). First, DPY30 controls *MYC* expression (28, 31). Second, DPY30 regulates the efficient binding of MYC oncoprotein to its genomic targets. This advances our understanding from mainly correlative observations to a functional role of H3K4 methylation for efficient MYC binding to the genome. By inhibiting the crucial activity of the MYC oncoprotein, targeting DPY30 might offer an alternative strategy for treating cancers that evade the inhibition of *MYC* expression following other treatments, such as the impressive BET protein inhibitors that repress *MYC* expression (55) but can induce resistant cancer cells with restored *MYC* expression (56, 57).

Our results show divergent effects of DPY30 reduction on MYC-mediated gene expression in both P493-6 and splenic B cells, reminiscent of the divergent impact on the induction and suppression of transcription changes during retinoid acid-mediated differentiation of mouse embryonic stem cells (27).

It has been a long-standing observation that despite the prevalent association of active chromatin marks with transcription, perturbing active chromatin marks can lead to expression changes of target genes in both directions. The underlying mechanisms remain poorly understood other than the common interpretation of indirect effects. Our results here suggest that DPY30 and efficient H3K4 methylation may help maintain a promoter environment more accessible for the binding of transcription factors to exert either an activating or repressing effect, rather than strictly promoting active transcription. This mechanism may be applicable to other chromatin modulators as well.

The precise molecular mechanisms by which DPY30 regulates the genomic binding of MYC remains unclear. Although H3K4 methylation is generally thought to be a permissive chromatin mark, direct measurement of chromatin accessibility change upon perturbation of this modification has to our knowledge not been reported. Our results suggest that DPY30 and efficient H3K4 methylation are important for maintaining the high chromatin accessibility of tested loci, and thus provide a possible mechanism for their role in the genomic binding of Myc. A quantitative assessment of genome-wide chromatin accessibility was unsuccessful due to difficulty of normalization across samples in which signals throughout the genome are likely to be affected (thus lacking the internal reference loci), and should be strengthened in the future to address this important mechanistic question. A general impact on chromatin accessibility may suggest that DPY30 level likely regulates binding of transcription factors beyond MYC, which is supported by our previous finding that Dpy30 is important for exogenous Oct4 to bind to its chromatin targets during cellular reprogramming (30). However, being a non-pioneer factor (13, 58), MYC is probably exceptionally dependent on the permissive chromatin environment facilitated by high DPY30 level.

Although DPY30 is not essential for the integrity of the SET1/MLL complexes (59) and does not directly bind MYC, we cannot exclude the possibility that DPY30 reduction may indirectly affect the binding of MYC with ASH2L, WDR5, or BPTF. These proteins physically associate with DPY30 (15) and regulate genomic binding of MYC (60, 61). Although a previous work showed that modest depletion of ASH2L did not affect genomic binding of MYC to a few target genes (39), we found here that ASH2L KD reduced MYC binding at many gene loci (Supplemental Figure 8C). Interestingly, while DPY30 KD had a stronger effect than ASH2L KD on MYC binding throughout these loci, a stronger effect on H3K4me3 at these loci was from ASH2L KD. These results suggest that DPY30 likely regulates genomic recruitment of MYC in part via its role in ASH2L-SET1/MLL complexes and also in part via its interaction with other factors, such as BPTF in the NURF chromatin-remodeling complex (15). The general importance of the core subunits of the SET1/MLL complexes in promoting the binding of MYC to its genomic targets may underlie their general role in oncogenesis, befitting their frequent amplification in cancers. In addition to regulating Myc binding to genome, DPY30 and H3K4 methylation can modulate the recruitment of H3K4 methylation readers (62) to regulate transcription of both MYC or non-MYC targets. Moreover, DPY30 may directly regulate the recruitment of BPTF and NURF complex via physical association (15, 63). Indeed, some genes that are not Myc targets were also altered in the *Eμ-Myc; Dpy30*$^{+/-}$ compared to *Eμ-Myc* B cells (Supplemental Figure 11), and may also contribute to their reduced tumorigenesis.

A high Dpy30 level ensures sufficient expression of a subset of pro-survival genes to counteract the apoptotic effects brought by the oncogenic assault. We show that the expression of *Mt1* and *Bcl-xL*, but not *Bcl2*, is significantly downregulated in *Eμ-Myc; Dpy30*$^{+/-}$ compared to the *Eμ-Myc* littermate B cells. Considering the specific requirement of endogenous *Bcl-xL* (64), but not *Bcl2* (65), for Myc-driven lymphomagenesis in mice, these results suggest a possible functional contribution of *Bcl-xL* regulation by Dpy30 in Myc-driven lymphomagenesis.

The role of high Dpy30 level in combating apoptotic stress is also seen in primary MEFs following oncogene transduction. In the BL cell model, P493-6 cells, however, DPY30 primarily promotes MYC-driven proliferation with little effect on apoptosis. This is likely a collective result of the modest downregulation of several proliferation-related genes (Supplemental Figure 5E). *CCNA2* and *MCM10*

have either unaffected MYC binding or very little MYC binding (Supplemental Figure 5F), and their downregulation by DPY30 KD may be a direct consequence of reduction of H3K4 methylation, presumably followed by reduced recruitment of H3K4 methylation readers involved in transcription (62) as discussed above. These results suggest that DPY30, being a global epigenetic modulator, can exhibit differential impacts on functional targets in different cellular systems.

Our data overall support a notion that the prominent epigenetic pathway of H3K4 methylation may be hijacked by oncogenes to promote tumorigenesis. Meanwhile, hyperactivation of oncogenes such as MYC renders tumor cells more dependent than normal cells on DPY30 (and likely other core subunits of the SET1/MLL complexes) for survival. Such a differential dependence provides a basis of the increasingly observed but poorly understood "epigenetic vulnerability" of certain cancers (66), which can be exploited for potential cancer treatment.

METHODS

Cell culture, gene knockdown (KD), growth, and transformation assays

P493-6 cells (37) were a kind gift from Alanna Ruddell (Fred Hutchinson Cancer Research Center, Seattle) with the permission of Dirk Eick (Helmholtz Center Munich, Germany). Raji and Jurkat cells were a kind gift from Tim Townes (University of Alabama at Birmingham). All these cells were cultured in RPMI 1640 medium with 10% fetal bovine serum (FBS). Primary mouse embryonic fibroblasts (MEFs) were isolated from E13.5 embryos, cultured in MEF culture medium (Dulbecco's Modified Eagle Medium [DMEM] supplemented with L-glutamine, 10% FBS, 0.1 mM non-essential amino acids, and 55μM β-mercaptoethanol, all from Invitrogen), and passage was kept at minimum. Transformations were performed on early passage cells (P3 or earlier). Retroviral particles were produced by transfecting 293T cells with pWZL-c-Myc-bsd (Addgene Plasmid #10674) or pBabe-HRas-V12-puro (Addgene #1768) and an ecotropic packaging vector using Polyethylenimine (PEI) Transfection Reagent (Polysciences Inc.). Viral supernatants were filtered through a 0.45 μM filter. MEFs were infected with HRAS-V12 and C-MYC viral particles followed by selection in puromycin (2 μg/ml) and blasticidin (2 μg/ml). Soft agar colony formation assays were performed by plating transformed MEFs in a 24-well plate at 2,000 cells/well. MEFs were cultured in a layer of MEF culture medium in 0.3% agar over a base layer composed of culture media in 0.6% agar and fed every 4 days. Colonies were formed over the course of 3-4 weeks. For stable KD, P493-6 cells or MEFs were infected with lentiviruses expressing control or DPY30 shRNAs [all sequences are available in (28)], followed by puromycin (2 μg/ml) selection for 2–3 days starting from 2 days after infection. Growth assays were performed in the absence of selecting antibiotics to avoid possible effect by differential expression of antibiotics-resistance gene. P493-6 cell growth was measured by manual counting, and the MEF cell growth was determined by CellTiter 96® AQueous One Solution Cell Proliferation Assay (Promega G3580).

Mice and tumor analyses

All mice were maintained under specific pathogen-free conditions and housed in individually ventilated cages. The *Dpy30*$^{+/-}$ mouse was generated in our laboratory before, and the genomic PCR assays and the primers used were reported (31). *Eμ-Myc* mice were purchased from the Jackson Laboratory (Stock No. 002728). Breeding was set up to obtain WT, *Dpy30*$^{+/-}$, *Eμ-Myc,* and *Eμ-Myc; Dpy30*$^{+/-}$ littermate mice. Peripheral blood profiles were measured using Hemavet 950 (DREW Scientific Inc.). Mice were monitored for illness and tumor development. Terminally sick mice were humanely sacrificed, and tumors were collected and stored at -80°C for later analyses. Survival was analyzed using the Prism software (GraphPad). For xenograft of MEFs, transduced MEFs (2 x 10^6 cells in 100 μl) were subcutaneously

injected into the flanks of 8-week-old male NSG mice (NOD.Cg-*Prkdc*^{scid} *Il2rg*^{tm1Wjl}/SzJ, purchased from the Jackson Laboratory, Stock No. 005557). Two weeks later, tumors were collected and weighed.

More Methods are in Supplemental Information.

Statistics

Unless indicated in the figure legends, the unpaired 2-tailed Student's t-test was used to calculate P values and evaluate the statistical significance of the difference between indicated samples. A P value less than 0.05 was considered significant. Four groups comparison was analyzed by one-factor or two-factor ANOVA as indicated in figure legends. If ANOVA was overall significant, post hoc *t* test was used for pairwise comparisons.

Study Approval

All animal procedures were approved by the Institutional Animal Care and Use Committee at the University of Alabama at Birmingham.

Accession Codes

All of the microarray, ChIP-seq, and RNA-seq data sets have been deposited in Gene Expression Omnibus database with the accession number GSE101854.

ACKNOWLEDGEMENTS

We thank Dirk Eick and Alanna Ruddell for providing the P493-6 cells, Tim Townes for providing the Raji and Jurkat cells, and the Comprehensive Flow Cytometry Core (CFCC) at UAB, which are supported by NIH core grants P30 AR048311 and P30 AI027767. We thank Ying Gai Tusing and Yanfang Zhao for technical assistance with mice work. This work was supported by American Cancer Society Research Scholar Award 128609-RSG-15-166-01-DMC, Start-up funds from the State of Alabama and University of Virginia, an internal fund from UAB, and NIH grant R01DK105531. HJ is a recipient of American Society of Hematology Scholar Award.

AUTHOR CONTRIBUTIONS

Z.Y. and K.S. conducted most of the experiments, T.B. and W.L. conducted some of the experiments, K.G and A.K. conducted bioinformatic analyses, H.J, Z.Y., K.S., and T.B. designed the experiments, and H.J. wrote the paper.

REFERENCES

1. Dang CV. MYC on the path to cancer. *Cell.* 2012;149(1):22-35.
2. Dalla-Favera R, Bregni M, Erikson J, Patterson D, Gallo RC, and Croce CM. Human c-myc onc gene is located on the region of chromosome 8 that is translocated in Burkitt lymphoma cells. *Proceedings of the National Academy of Sciences of the United States of America.* 1982;79(24):7824-7.
3. Taub R, Kirsch I, Morton C, Lenoir G, Swan D, Tronick S, et al. Translocation of the c-myc gene into the immunoglobulin heavy chain locus in human Burkitt lymphoma and murine plasmacytoma cells. *Proceedings of the National Academy of Sciences of the United States of America.* 1982;79(24):7837-41.
4. Adams JM, Harris AW, Pinkert CA, Corcoran LM, Alexander WS, Cory S, et al. The c-myc oncogene driven by immunoglobulin enhancers induces lymphoid malignancy in transgenic mice. *Nature.* 1985;318(6046):533-8.
5. Rounbehler RJ, Fallahi M, Yang C, Steeves MA, Li W, Doherty JR, et al. Tristetraprolin impairs myc-induced lymphoma and abolishes the malignant state. *Cell.* 2012;150(3):563-74.
6. Barna M, Pusic A, Zollo O, Costa M, Kondrashov N, Rego E, et al. Suppression of Myc oncogenic activity by ribosomal protein haploinsufficiency. *Nature.* 2008;456(7224):971-5.
7. Kress TR, Sabo A, and Amati B. MYC: connecting selective transcriptional control to global RNA production. *Nature reviews Cancer.* 2015;15(10):593-607.
8. Lin CY, Loven J, Rahl PB, Paranal RM, Burge CB, Bradner JE, et al. Transcriptional amplification in tumor cells with elevated c-Myc. *Cell.* 2012;151(1):56-67.
9. Nie Z, Hu G, Wei G, Cui K, Yamane A, Resch W, et al. c-Myc is a universal amplifier of expressed genes in lymphocytes and embryonic stem cells. *Cell.* 2012;151(1):68-79.
10. Sabo A, Kress TR, Pelizzola M, de Pretis S, Gorski MM, Tesi A, et al. Selective transcriptional regulation by Myc in cellular growth control and lymphomagenesis. *Nature.* 2014;511(7510):488-92.
11. Walz S, Lorenzin F, Morton J, Wiese KE, von Eyss B, Herold S, et al. Activation and repression by oncogenic MYC shape tumour-specific gene expression profiles. *Nature.* 2014;511(7510):483-7.
12. Guccione E, Martinato F, Finocchiaro G, Luzi L, Tizzoni L, Dall' Olio V, et al. Myc-binding-site recognition in the human genome is determined by chromatin context. *Nat Cell Biol.* 2006;8(7):764-70.
13. Soufi A, Donahue G, and Zaret KS. Facilitators and impediments of the pluripotency reprogramming factors' initial engagement with the genome. *Cell.* 2012;151(5):994-1004.
14. Schneider R, Bannister AJ, Myers FA, Thorne AW, Crane-Robinson C, and Kouzarides T. Histone H3 lysine 4 methylation patterns in higher eukaryotic genes. *Nat Cell Biol.* 2004;6(1):73-7.
15. Jiang H, Lu X, Shimada M, Dou Y, Tang Z, and Roeder RG. Regulation of transcription by the MLL2 complex and MLL complex-associated AKAP95. *Nat Struct Mol Biol.* 2013;20(10):1156-63.
16. Lauberth SM, Nakayama T, Wu X, Ferris AL, Tang Z, Hughes SH, et al. H3K4me3 interactions with TAF3 regulate preinitiation complex assembly and selective gene activation. *Cell.* 2013;152(5):1021-36.
17. Shilatifard A. The COMPASS Family of Histone H3K4 Methylases: Mechanisms of Regulation in Development and Disease Pathogenesis. *Annu Rev Biochem.* 2012;81:65-95.
18. Rao RC, and Dou Y. Hijacked in cancer: the KMT2 (MLL) family of methyltransferases. *Nature reviews Cancer.* 2015;15(6):334-46.
19. Okosun J, Bodor C, Wang J, Araf S, Yang CY, Pan C, et al. Integrated genomic analysis identifies recurrent mutations and evolution patterns driving the initiation and progression of follicular lymphoma. *Nature genetics.* 2014;46(2):176-81.

20. Parsons DW, Li M, Zhang X, Jones S, Leary RJ, Lin JC, et al. The genetic landscape of the childhood cancer medulloblastoma. *Science (New York, NY).* 2011;331(6016):435-9.
21. Pasqualucci L, Trifonov V, Fabbri G, Ma J, Rossi D, Chiarenza A, et al. Analysis of the coding genome of diffuse large B-cell lymphoma. *Nature genetics.* 2011;43(9):830-7.
22. Rabello Ddo A, de Moura CA, de Andrade RV, Motoyama AB, and Silva FP. Altered expression of MLL methyltransferase family genes in breast cancer. *International journal of oncology.* 2013;43(2):653-60.
23. Song Y, Li L, Ou Y, Gao Z, Li E, Li X, et al. Identification of genomic alterations in oesophageal squamous cell cancer. *Nature.* 2014;509(7498):91-5.
24. Luscher-Firzlaff J, Gawlista I, Vervoorts J, Kapelle K, Braunschweig T, Walsemann G, et al. The human trithorax protein hASH2 functions as an oncoprotein. *Cancer research.* 2008;68(3):749-58.
25. Kim JY, Banerjee T, Vinckevicius A, Luo Q, Parker JB, Baker MR, et al. A role for WDR5 in integrating threonine 11 phosphorylation to lysine 4 methylation on histone H3 during androgen signaling and in prostate cancer. *Molecular cell.* 2014;54(4):613-25.
26. Kandoth C, McLellan MD, Vandin F, Ye K, Niu B, Lu C, et al. Mutational landscape and significance across 12 major cancer types. *Nature.* 2013;502(7471):333-9.
27. Jiang H, Shukla A, Wang X, Chen WY, Bernstein BE, and Roeder RG. Role for Dpy-30 in ES Cell-Fate Specification by Regulation of H3K4 Methylation within Bivalent Domains. *Cell.* 2011;144(4):513-25.
28. Yang Z, Augustin J, Chang C, Hu J, Shah K, Chang CW, et al. The DPY30 subunit in SET1/MLL complexes regulates the proliferation and differentiation of hematopoietic progenitor cells. *Blood.* 2014;124(13):2025-33.
29. Simboeck E, Gutierrez A, Cozzuto L, Beringer M, Caizzi L, Keyes WM, et al. DPY30 regulates pathways in cellular senescence through ID protein expression. *The EMBO journal.* 2013;32(16):2217-30.
30. Yang Z, Augustin J, Hu J, and Jiang H. Physical Interactions and Functional Coordination between the Core Subunits of Set1/Mll Complexes and the Reprogramming Factors. *PloS one.* 2015;10(12):e0145336.
31. Yang Z, Shah K, Khodadadi-Jamayran A, and Jiang H. Dpy30 is critical for maintaining the identity and function of adult hematopoietic stem cells. *The Journal of experimental medicine.* 2016;213(11):2349-64.
32. Cerami E, Gao J, Dogrusoz U, Gross BE, Sumer SO, Aksoy BA, et al. The cBio cancer genomics portal: an open platform for exploring multidimensional cancer genomics data. *Cancer discovery.* 2012;2(5):401-4.
33. Hummel M, Bentink S, Berger H, Klapper W, Wessendorf S, Barth TF, et al. A biologic definition of Burkitt's lymphoma from transcriptional and genomic profiling. *The New England journal of medicine.* 2006;354(23):2419-30.
34. Saglio G, Emanuel BS, Guerrasio A, Giubellino MC, Serra A, Lusso P, et al. 3' c-myc rearrangement in a human leukemic T-cell line. *Cancer research.* 1986;46(3):1413-7.
35. Mu Q, Ma Q, Lu S, Zhang T, Yu M, Huang X, et al. 10058-F4, a c-Myc inhibitor, markedly increases valproic acid-induced cell death in Jurkat and CCRF-CEM T-lymphoblastic leukemia cells. *Oncology letters.* 2014;8(3):1355-9.
36. Amati B, Brooks MW, Levy N, Littlewood TD, Evan GI, and Land H. Oncogenic activity of the c-Myc protein requires dimerization with Max. *Cell.* 1993;72(2):233-45.
37. Pajic A, Spitkovsky D, Christoph B, Kempkes B, Schuhmacher M, Staege MS, et al. Cell cycle activation by c-myc in a burkitt lymphoma model cell line. *International journal of cancer Journal international du cancer.* 2000;87(6):787-93.
38. Cho YW, Hong T, Hong S, Guo H, Yu H, Kim D, et al. PTIP associates with MLL3- and MLL4-containing histone H3 lysine 4 methyltransferase complex. *J Biol Chem.* 2007;282(28):20395-406.

39. Ullius A, Luscher-Firzlaff J, Costa IG, Walsemann G, Forst AH, Gusmao EG, et al. The interaction of MYC with the trithorax protein ASH2L promotes gene transcription by regulating H3K27 modification. *Nucleic acids research.* 2014;42(11):6901-20.
40. Buenrostro JD, Giresi PG, Zaba LC, Chang HY, and Greenleaf WJ. Transposition of native chromatin for fast and sensitive epigenomic profiling of open chromatin, DNA-binding proteins and nucleosome position. *Nature methods.* 2013;10(12):1213-8.
41. Vafa O, Wade M, Kern S, Beeche M, Pandita TK, Hampton GM, et al. c-Myc can induce DNA damage, increase reactive oxygen species, and mitigate p53 function: a mechanism for oncogene-induced genetic instability. *Molecular cell.* 2002;9(5):1031-44.
42. Subramanian A, Tamayo P, Mootha VK, Mukherjee S, Ebert BL, Gillette MA, et al. Gene set enrichment analysis: a knowledge-based approach for interpreting genome-wide expression profiles. *Proceedings of the National Academy of Sciences of the United States of America.* 2005;102(43):15545-50.
43. Dutsch-Wicherek M, Sikora J, and Tomaszewska R. The possible biological role of metallothionein in apoptosis. *Frontiers in bioscience : a journal and virtual library.* 2008;13:4029-38.
44. Shimoda R, Achanzar WE, Qu W, Nagamine T, Takagi H, Mori M, et al. Metallothionein is a potential negative regulator of apoptosis. *Toxicological sciences : an official journal of the Society of Toxicology.* 2003;73(2):294-300.
45. Youle RJ, and Strasser A. The BCL-2 protein family: opposing activities that mediate cell death. *Nature reviews Molecular cell biology.* 2008;9(1):47-59.
46. Ernst P, and Vakoc CR. WRAD: enabler of the SET1-family of H3K4 methyltransferases. *Brief Funct Genomics.* 2012;11(3):217-26.
47. Lin DC, Hao JJ, Nagata Y, Xu L, Shang L, Meng X, et al. Genomic and molecular characterization of esophageal squamous cell carcinoma. *Nature genetics.* 2014;46(5):467-73.
48. Watanabe Y, Castoro RJ, Kim HS, North B, Oikawa R, Hiraishi T, et al. Frequent alteration of MLL3 frameshift mutations in microsatellite deficient colorectal cancer. *PloS one.* 2011;6(8):e23320.
49. Chen C, Liu Y, Rappaport AR, Kitzing T, Schultz N, Zhao Z, et al. MLL3 Is a Haploinsufficient 7q Tumor Suppressor in Acute Myeloid Leukemia. *Cancer cell.* 2014;25(5):652-65.
50. Zhang J, Dominguez-Sola D, Hussein S, Lee JE, Holmes AB, Bansal M, et al. Disruption of KMT2D perturbs germinal center B cell development and promotes lymphomagenesis. *Nature medicine.* 2015;21(10):1190-8.
51. Lee YJ, Han ME, Baek SJ, Kim SY, and Oh SO. Roles of DPY30 in the Proliferation and Motility of Gastric Cancer Cells. *PloS one.* 2015;10(7):e0131863.
52. Butler JS, Qiu YH, Zhang N, Yoo SY, Coombes KR, Dent SY, et al. Low expression of ASH2L protein correlates with a favorable outcome in acute myeloid leukemia. *Leukemia & lymphoma.* 2017;58(5):1207-18.
53. Sun Y, Bell JL, Carter D, Gherardi S, Poulos RC, Milazzo G, et al. WDR5 Supports an N-Myc Transcriptional Complex That Drives a Protumorigenic Gene Expression Signature in Neuroblastoma. *Cancer research.* 2015;75(23):5143-54.
54. Carugo A, Genovese G, Seth S, Nezi L, Rose JL, Bossi D, et al. In Vivo Functional Platform Targeting Patient-Derived Xenografts Identifies WDR5-Myc Association as a Critical Determinant of Pancreatic Cancer. *Cell reports.* 2016;16(1):133-47.
55. Shi J, and Vakoc CR. The mechanisms behind the therapeutic activity of BET bromodomain inhibition. *Molecular cell.* 2014;54(5):728-36.
56. Rathert P, Roth M, Neumann T, Muerdter F, Roe J-S, Muhar M, et al. Transcriptional plasticity promotes primary and acquired resistance to BET inhibition. *Nature.* 2015;525(7570):543-7.
57. Fong CY, Gilan O, Lam EYN, Rubin AF, Ftouni S, Tyler D, et al. BET inhibitor resistance emerges from leukaemia stem cells. *Nature.* 2015;525(7570):538-42.

58. Soufi A, Garcia MF, Jaroszewicz A, Osman N, Pellegrini M, and Zaret KS. Pioneer transcription factors target partial DNA motifs on nucleosomes to initiate reprogramming. *Cell.* 2015;161(3):555-68.
59. Dou Y, Milne TA, Ruthenburg AJ, Lee S, Lee JW, Verdine GL, et al. Regulation of MLL1 H3K4 methyltransferase activity by its core components. *Nat Struct Mol Biol.* 2006;13(8):713-9.
60. Thomas LR, Wang Q, Grieb BC, Phan J, Foshage AM, Sun Q, et al. Interaction with WDR5 promotes target gene recognition and tumorigenesis by MYC. *Molecular cell.* 2015;58(3):440-52.
61. Richart L, Carrillo-de Santa Pau E, Rio-Machin A, de Andres MP, Cigudosa JC, Lobo VJ, et al. BPTF is required for c-MYC transcriptional activity and in vivo tumorigenesis. *Nature communications.* 2016;7:10153.
62. Ruthenburg AJ, Allis CD, and Wysocka J. Methylation of lysine 4 on histone H3: intricacy of writing and reading a single epigenetic mark. *Mol Cell.* 2007;25(1):15-30.
63. Tremblay V, Zhang P, Chaturvedi CP, Thornton J, Brunzelle JS, Skiniotis G, et al. Molecular Basis for DPY-30 Association to COMPASS-like and NURF Complexes. *Structure (London, England : 1993).* 2014;22(12):1821-30.
64. Kelly PN, Grabow S, Delbridge AR, Strasser A, and Adams JM. Endogenous Bcl-xL is essential for Myc-driven lymphomagenesis in mice. *Blood.* 2011;118(24):6380-6.
65. Kelly PN, Puthalakath H, Adams JM, and Strasser A. Endogenous bcl-2 is not required for the development of Emu-myc-induced B-cell lymphoma. *Blood.* 2007;109(11):4907-13.
66. Dawson MA, and Kouzarides T. Cancer epigenetics: from mechanism to therapy. *Cell.* 2012;150(1):12-27.

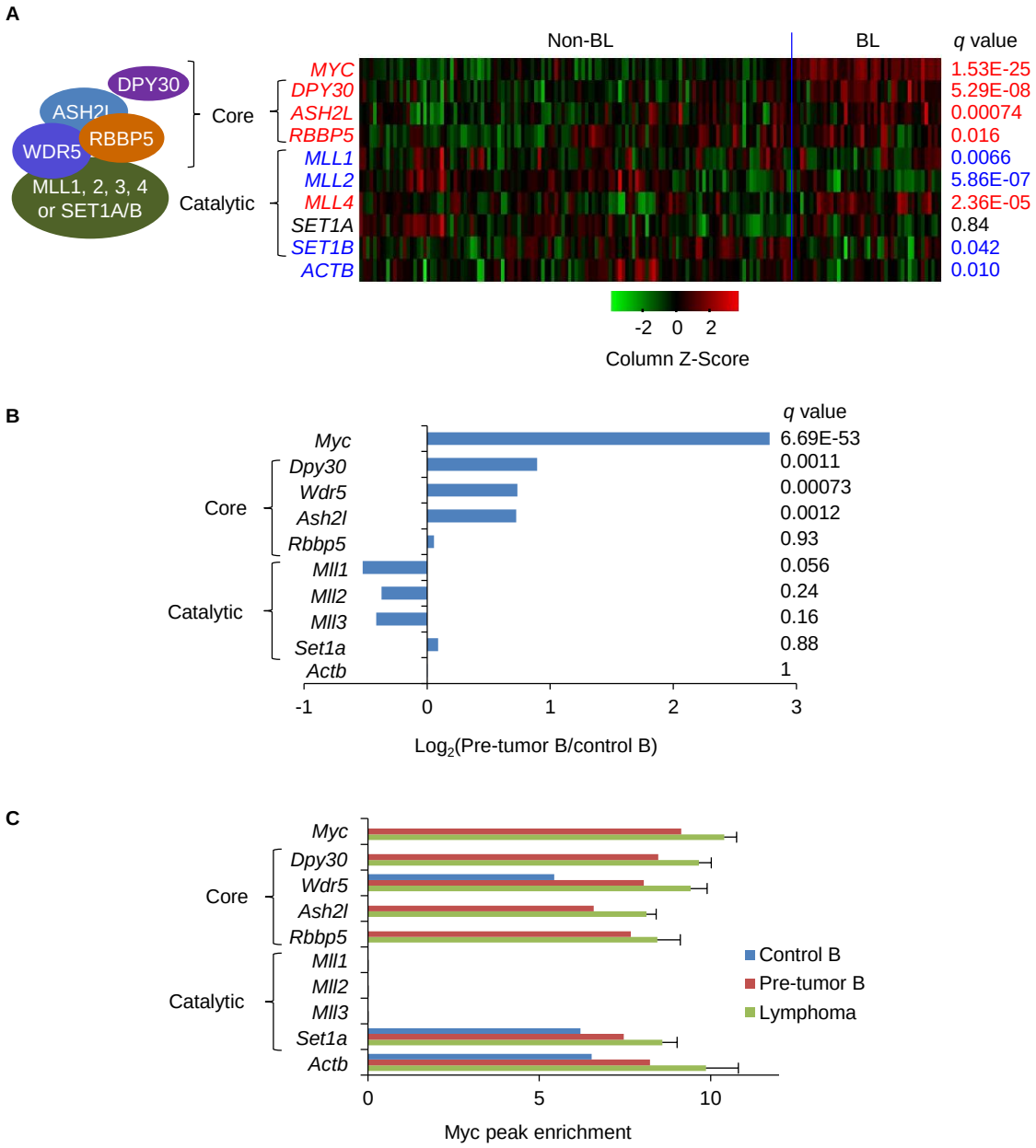

Figure 1. MYC directly promotes the expression of core subunits in SET1/MLL complexes. (A) Expression of SET1/MLL complex subunits in 44 primary human BL vs. 129 non-BL samples from GSE4475. Each column represents a sample and each row represents the indicated gene. Genes in red indicate increased expression in BL, and genes in blue indicate decreased expression in BL. q values (false discovery rates) of the expression changes between non-BL and BL samples are listed on the right. The color key at the bottom reflects expression level. **(B-C)** Analyses of data from *Eμ-Myc* mice from GSE51011. **(B)** Expression change of Set1/Mll complex subunits from non-transgenic control B cells to pre-tumor B cells in young *Eμ-Myc* mice**.** q values (false discovery rates) of the expression changes between 4 pre-tumor and 4 control samples are listed on the right. **(C)** Myc binding to genes encoding Set1/Mll complex subunits in indicated samples, shown by Myc ChIP signal peak enrichment values (mean +SD) at the promoters of indicated genes from one control, one pre-tumor, and 3 tumor samples.

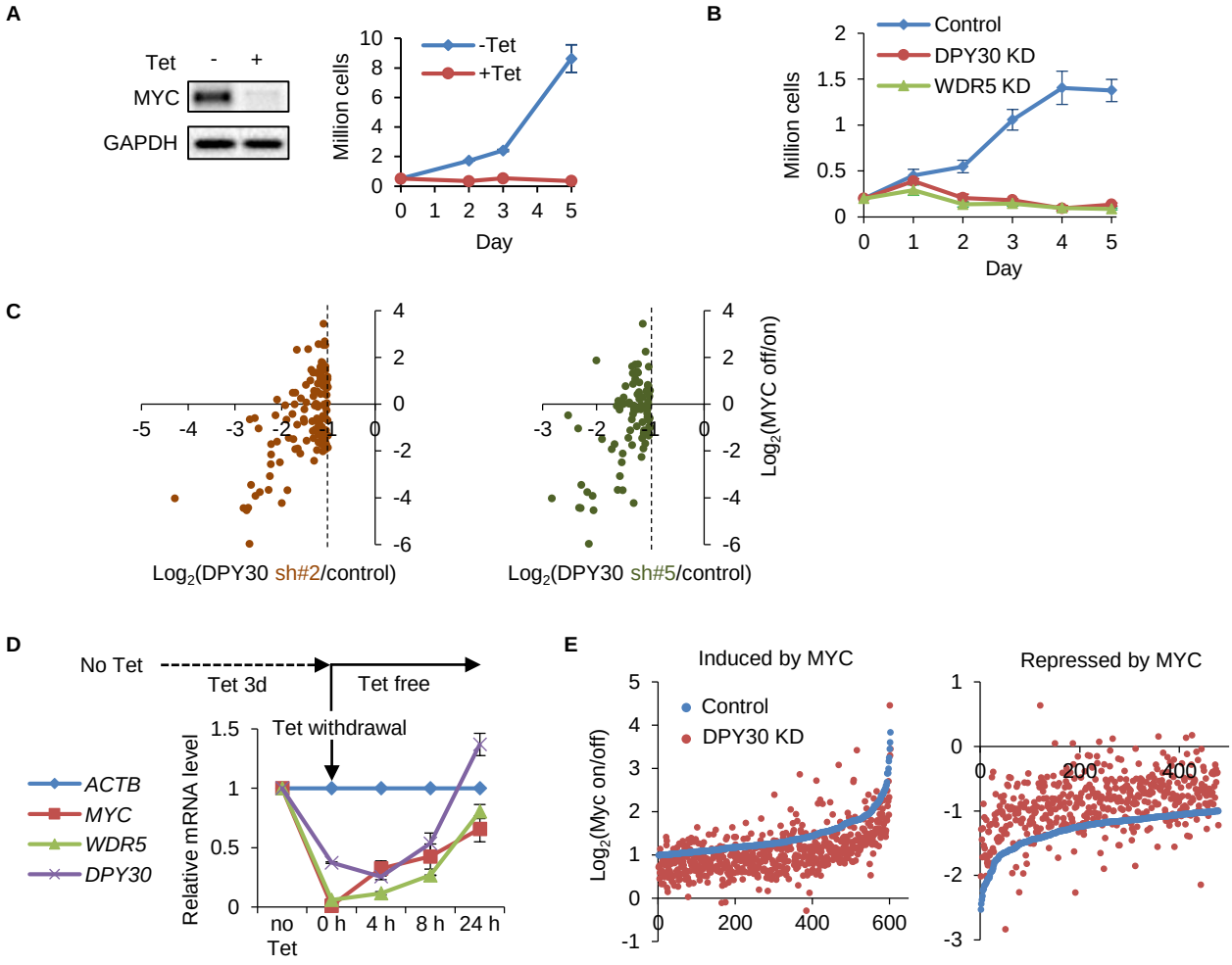

Figure 2. Dpy30 regulates expression of *MYC* and MYC targets. (A) Left, immunoblotting showing MYC silencing by tetracycline. Right, growth curves of P493-6 cells in the presence/absence of tetracycline. Cell numbers and mean ± SD from two independent platings are plotted. **(B)** Growth of P493-6 cells following DPY30 or WDR5 KD. Cell numbers were counted and mean ± SD from eight independent measurements are plotted, from a representative assay out of >8 (for Dpy30 KD) or >4 (for Wdr5 KD) independent knockdown and growth assays. **(C)** Co-dependence of many genes on DPY30 and MYC. P493-6 cells were either depleted of DPY30 by one of two different shRNAs (sh#2 and sh#5) or cultured with tetracycline for 3 days to turn off *MYC*, and the expression changes were analyzed by microarray. For genes downregulated over 2 fold by DPY30 KD using each shRNA, logarithmic fold changes of gene expression upon DPY30 KD are plotted against their expression changes after turning *MYC* off. Each dot represents a gene. **(D)** P493-6 cells were cultured in the presence of tetracycline for 3 days, followed by tetracycline withdrawal and culture in tetracycline-free medium. Relative mRNA levels of indicated genes at different time points were determined by qPCR and normalized to *ACTB*, shown as mean ± SD from duplicate measurements representative of two independent assays. **(E)** Control (Scramble shRNA) and DPY30 KD P493-6 cells were treated with the scheme in (D), and cells at 0h and 4h after tetracycline withdrawal were used for microarray analyses. Logarithmic fold changes from 0h to 4h (from MYC off to 4 hours of MYC reactivation) are plotted for the genes upregulated over 2 fold in control cells (left) and genes downregulated over 2 fold in control cells (right). Each dot represents a gene.

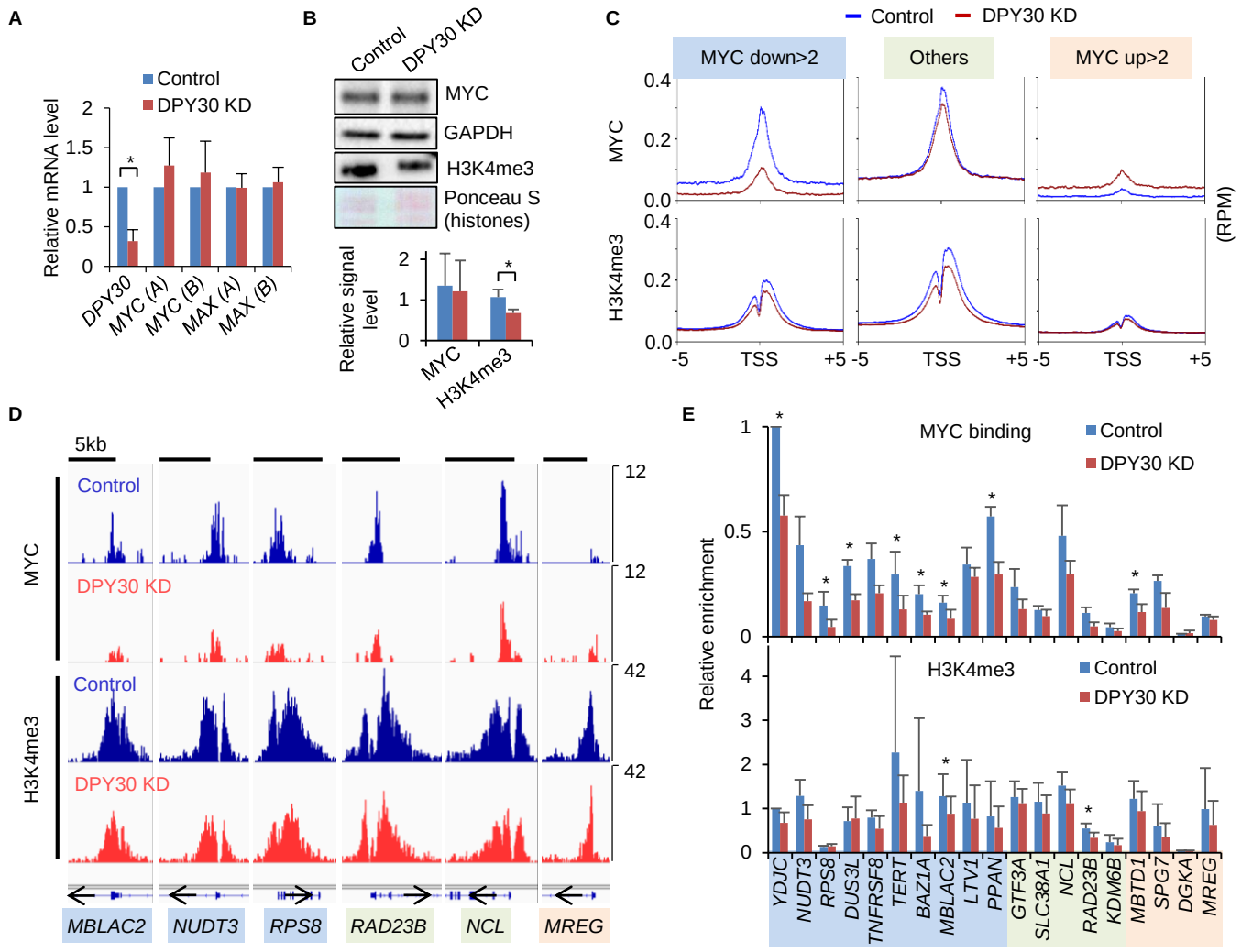

Figure 3. DPY30 is important for efficient binding of MYC to its genomic loci. (A) *DPY30*, *MYC,* and *MAX* mRNA levels were determined by qPCR using two different primers for *MYC* and *MAX* and normalized to *ACTB* from 5 independent knockdown assays in P493-6 cells. **(B)** Top, total cell lysates from control and DPY30 KD P493-6 cells were used for immunoblotting by indicated antibodies and for Ponceau S staining of histones. Bottom, relative signal intensity was calculated as a ratio over GAPDH (for MYC) or histones (for H3K4me3) from 3 samples each. **(C and D)** Analyses of ChIP-seq from control and DPY30 KD P493-6 cells. **(C)** Composite profiles of MYC ChIP signals (top) at TSSs are grouped (and color coded) by the fold change upon DPY30 KD in P493-6 cells. There are 9233, 9457, and 33451 genes where MYC binding was reduced over 2 fold (MYC down >2), increased over 2 fold (MYC up >2), and changed less than 2 fold in either direction (Others), respectively. The corresponding H3K4me3 ChIP signals (bottom) are also shown for each group of genes. **(D)** MYC and H3K4me3 ChIP-seq profiles for representative genes within each group shown in (C). **(E)** Multiple genes within each group shown in (C) were validated for MYC and H3K4me3 ChIP at TSSs by qPCR, calculated from the ratio of the percent input value for each locus over that for the *YDJC* site in the control sample from 3 independent knockdown and ChIP assays in P493-6 cells. Results of individual repeats are also shown in Supplemental Figure 7. Data represent the mean + SD (A, B, and E). *P < 0.05 by Student's t test.

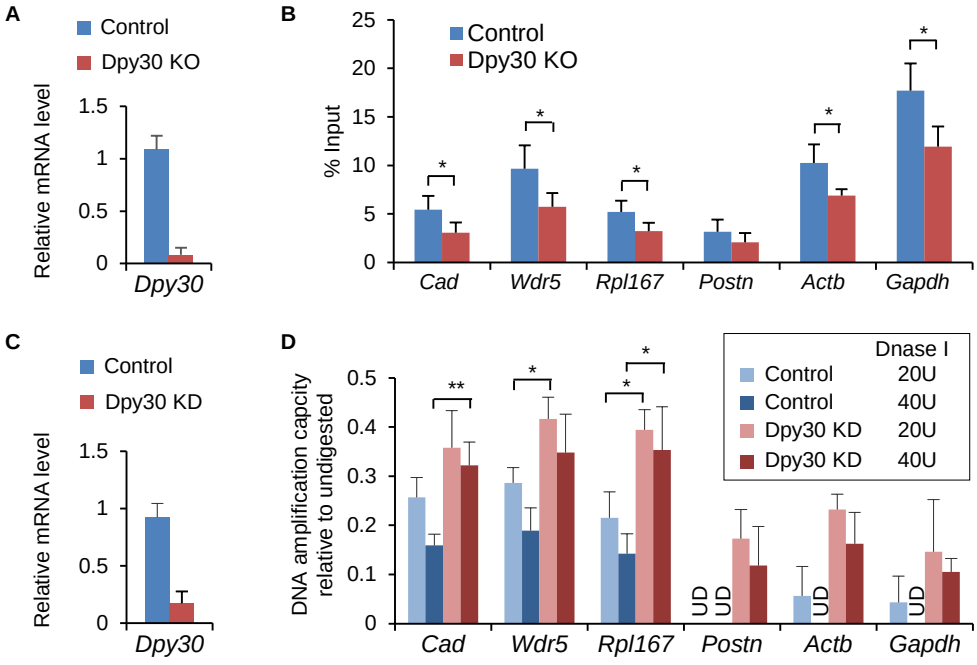

Figure 4. Dpy30 regulates chromatin accessibility. **(A-B)** Primary MEFs derived from *Dpy30*$^{F/F}$ (control) or *CAG-CreER; Dpy30*$^{F/F}$ (KO) were treated with 4-hydroxytamoxifen for 4 days, followed by qPCR assays for relative mRNA levels of *Dpy30* which was normalized to *Gapdh* **(A),** and ATAC-qPCR assays **(B)**. Results are from 4 independent 4-hydroxytamoxifen treatments followed by ATAC-qPCR assays. Related information is also in Supplemental Figure 9B. **(C and D)** Relative mRNA levels of *Dpy30* normalized to *Gapdh* **(C)** and DNase I hypersensitivity assays **(D)** in MEFs expressing scramble (control) or Dpy30 shRNA (KD). Results are shown as mean +SD of triplicate measurements. In **(D)**, DNAs after digestion of 0, 20, or 40 units/ml of Dnase I were used for amplification of indicated loci, and the amplification capacity of the digested samples relative to the undigested sample (set to 1 for both control and KD) was determined from triplicate measurements. Note that the higher the value, the more abundant the amplifiable DNA was left after digestion, indicating less accessible chromatin. UD, undetectable by qPCR (suggesting high accessibility and complete digestion). Data represent the mean + SD. **P* < 0.05, ***P* < 0.01 by Student's *t* test (B) and one-factor ANOVA with post hoc *t* test (D).

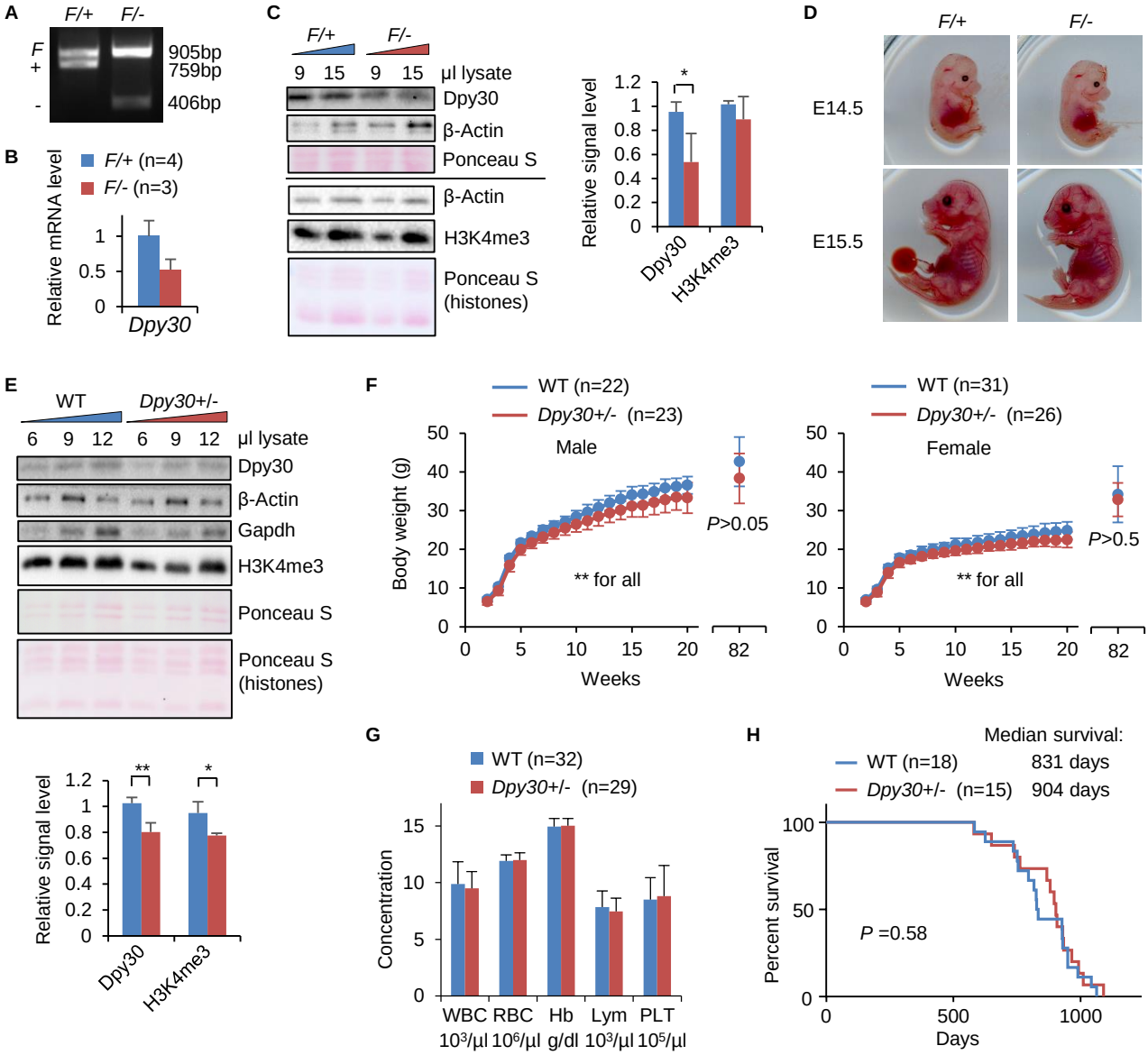

Figure 5. Full level of Dpy30 is dispensable for normal physiology of mice. (A) Genomic PCR results to detect *Dpy30* deletion in fetal livers of *Dpy30*$^{F/+}$ and *Dpy30*$^{F/-}$ mice. The "*F*" allele is the floxed (conditional) allele. The calculated sizes of the PCR products are shown on the right. **(B)** Relative mRNA levels of *Dpy30* were determined by qPCR and normalized to *Actb* from *Dpy30*$^{F/+}$ and *Dpy30*$^{F/-}$ fetal livers derived from indicated numbers of E14.5 littermate embryos. **(C)** Left, immunoblotting for indicated proteins (or modification) with increasing loading doses of lysates from fetal livers of *Dpy30*$^{F/+}$ and *Dpy30*$^{F/-}$ E14.5 littermate embryos. Ponceau S stainings of irrelevant proteins and histones are also shown. Right, relative signal intensity was calculated as a ratio over histones from 3 samples for each genotype at a single loading dose. **(D)** Gross morphology of *Dpy30*$^{F/+}$ and *Dpy30*$^{F/-}$ embryos at E14.5 and E15.5. **(E)** Left, immunoblotting for indicated proteins (or modification) with increasing loading doses of lysates from splenic B cells of 4-week old WT and *Dpy30*$^{+/-}$ littermate mice. Ponceau S stainings of irrelevant proteins and histones are also shown. Bottom, relative signal intensity was calculated the same ways as (C). **(F)** Body weight curves. Numbers of animals are indicated for all time points on top except for week 82, when male WT, n = 13; male *Dpy30*$^{+/-}$, n = 15; female WT, n = 12; female *Dpy30*$^{+/-}$, n = 7. **(G)** Peripheral blood cell and hemoglobin (Hb) concentrations of 8-week old littermates. **(H)** Kaplan-Meier curves. Data represent the mean + SD (B, C, E and G) or ± SD (F). **P* < 0.05 and ***P* < 0.01 by Student's *t*-test (C, right, and F, for each pair at each time points). *P* value in (H) was calculated by log-rank test.

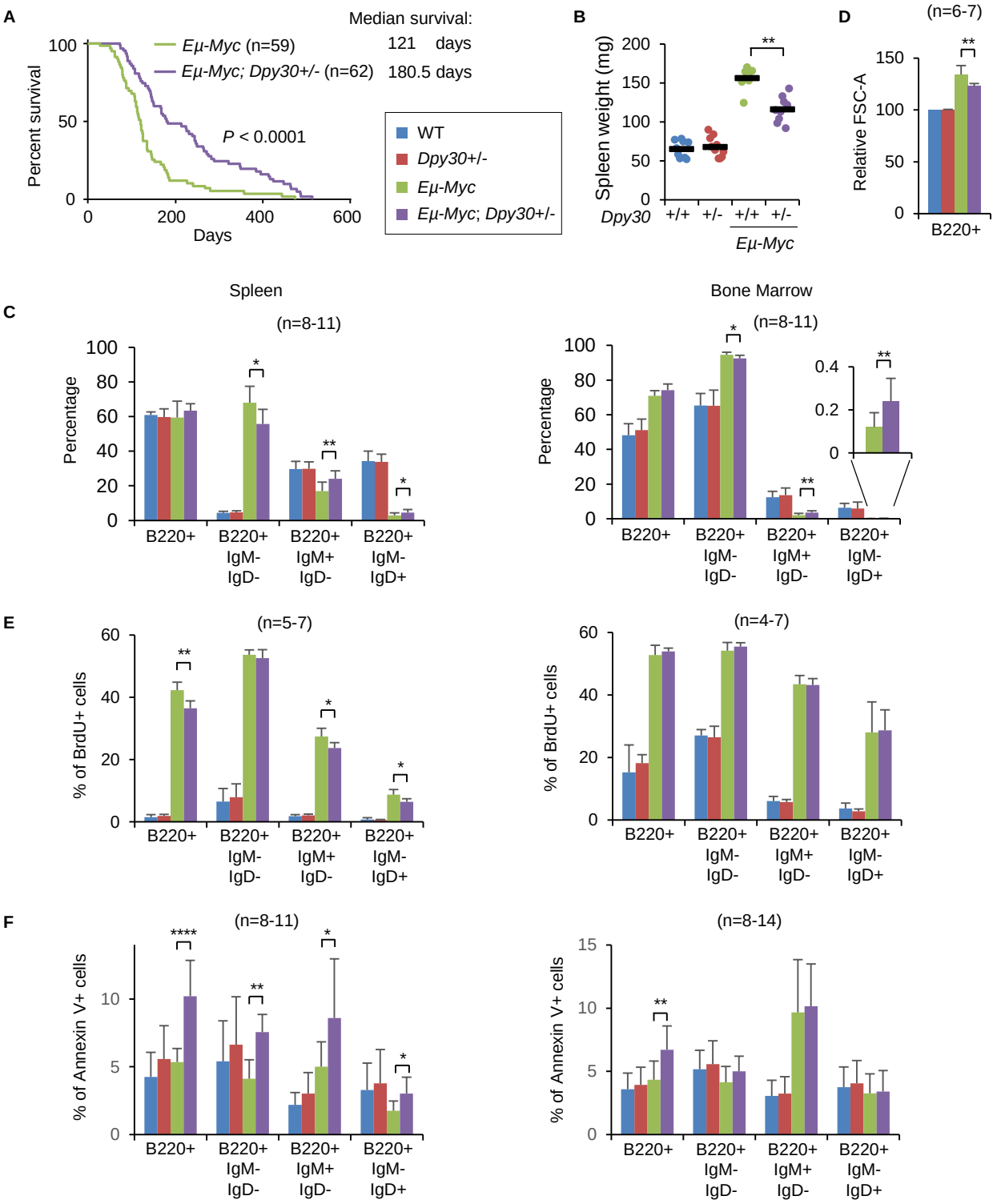

Figure 6. *Dpy30* heterozygosity suppresses Myc-driven lymphomagenesis in mice. (A) Kaplan-Meier curves. Median survival times are indicated. The color legends apply to all panels. **(B)** Spleen weight of 4-week old littermates. Each dot represents an animal. WT, n = 9; *Dpy30*$^{+/-}$, n = 10; *Eμ-Myc*, n = 7; and *Eμ-Myc; Dpy30*$^{+/-}$, n = 9. **(C)** Percentages of the B220^{+} cells in total cells or percentages of the subpopulations in all B220^{+} cells. For spleen and BM each, WT, n = 8; *Dpy30*$^{+/-}$, n = 11; *Eμ-Myc*, n = 11; and *Eμ-Myc; Dpy30*$^{+/-}$, n = 8. **(D)** Sizes of spleen B220^{+} cells as shown by the FSC-A values in FACS analysis. WT, n = 6; *Dpy30*$^{+/-}$, n = 6; *Eμ-Myc*, n = 7; and *Eμ-Myc; Dpy30*$^{+/-}$, n = 7. **(E)** BrdU staining of spleen and BM cells with indicated cell surface markers after in vivo BrdU labeling. For spleen, WT, n = 5; *Dpy30*$^{+/-}$, n = 7; *Eμ-Myc*, n = 5; and *Eμ-Myc; Dpy30*$^{+/-}$, n = 5. For BM, WT, n = 4; *Dpy30*$^{+/-}$, n = 7; *Eμ-Myc*, n = 5; and *Eμ-Myc; Dpy30*$^{+/-}$, n = 5. **(F)** Annexin V staining of spleen and BM cells with indicated cell surface markers. For spleen, WT, n = 8; *Dpy30*$^{+/-}$, n = 11; *Eμ-Myc*, n = 11; and *Eμ-Myc; Dpy30*$^{+/-}$, n = 8. For BM, WT, n = 8; *Dpy30*$^{+/-}$, n = 11; *Eμ-Myc*, n = 14; and *Eμ-Myc; Dpy30*$^{+/-}$, n = 10. Data represent the mean + SD (C-F). *P < 0.05, **P < 0.01, and ****P < 0.0001 by log-rank test (A) and one-factor ANOVA with post hoc *t* test (B-F).

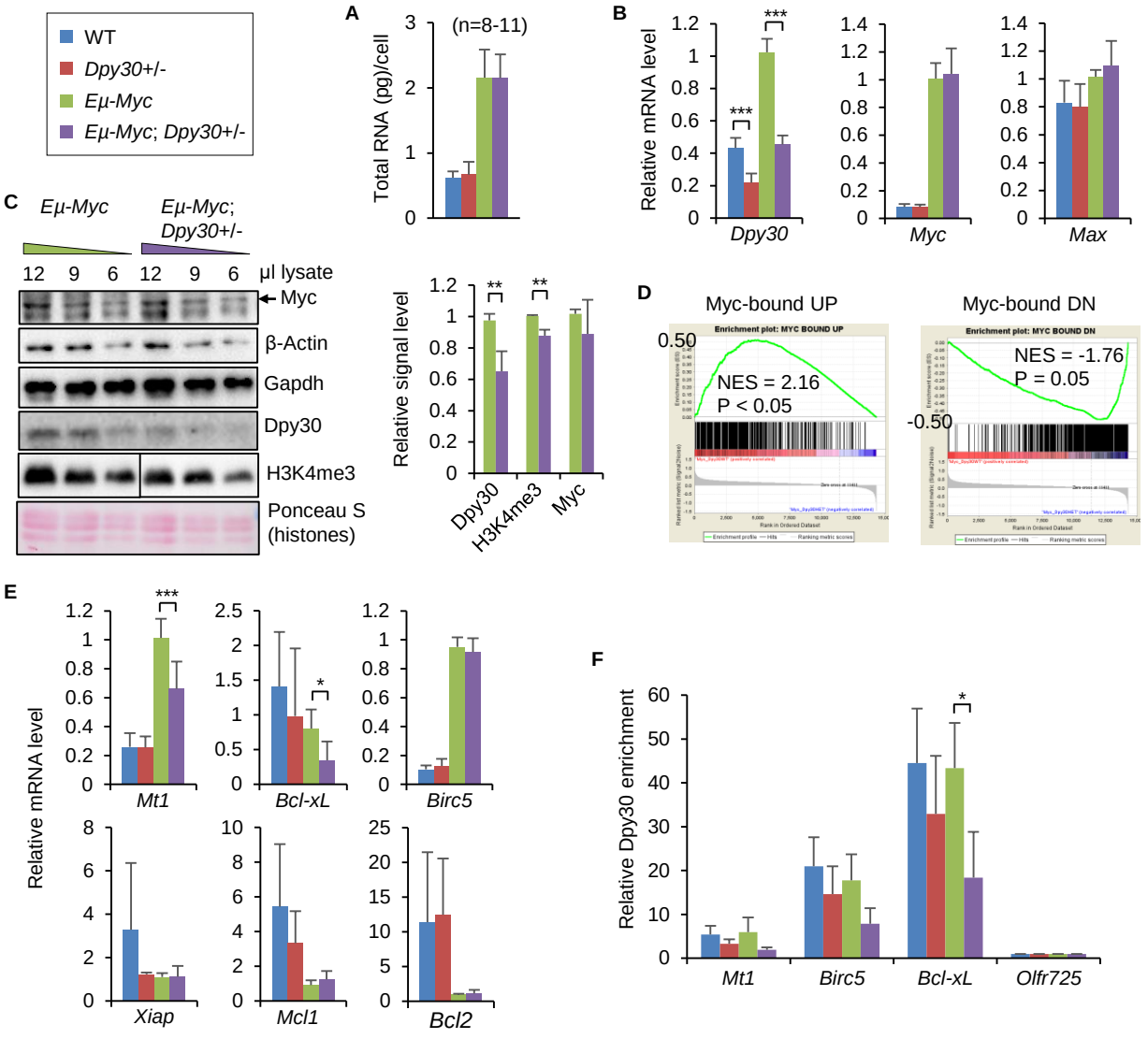

Figure 7. Impact of *Dpy30* heterozygosity on gene expression in splenic B cells. All data are from purified splenic B220$^+$ cells. Color legends apply for all panels. **(A)** Total RNA levels per cell from: WT, n = 8; *Dpy30*$^{+/-}$, n = 1; *Eμ-Myc*, n = 9; and *Eμ-Myc; Dpy30*$^{+/-}$, n = 11. **(B and E)** Relative mRNA levels of indicated genes were determined by qPCR and normalized to *Actb*, shown as mean + SD from 6, 6, 8, and 6 mice (for *Dpy30* and *Myc* in B, and *Bcl2*, *Bcl-xL*, and *Birc5* in E), 5, 4, 9, and 9 mice (for *Max* in B and *Mt1* in E), or 3, 3, 5, 3 mice (for *Xiap* and *Mcl1* in E) with WT, *Dpy30*$^{+/-}$, *Eμ-Myc*, and *Eμ-Myc; Dpy30*$^{+/-}$ genotypes, respectively. **(C)** Left, immunoblotting for indicated proteins (or modification) with increasing loading doses of lysates. Right, relative signal intensity was calculated as a ratio over β-Actin, and plotted from 3 *Eμ-Myc* or 4 *Eμ-Myc; Dpy30*$^{+/-}$ samples at a single dose of loading. $^{**}P < 0.01$. **(D)** GSEA for the Myc-bound gene sets comparing gene expression profiles of *Eμ-Myc* and *Eμ-Myc; Dpy30*$^{+/-}$ B cells. Myc targets that are most significantly up- (Myc-bound UP) or down-regulated (Myc-bound DN) by Myc (curated from GSE51011, see Methods and Supplemental Table 4) were used as gene sets, respectively. **(F)** Relative Dpy30 enrichment at indicated gene TSSs were determined by Dpy30 ChIP on purified B220$^+$ cells, calculated from the ratio of the percent input value for each locus over that for the negative control site (*Olfr725*) in the *Eμ-Myc* sample from 3 mice of each genotype. Data represent the mean + SD. $^{*}P < 0.05$, $^{**}P < 0.01$, $^{***}P < 0.001$ by Student's *t*-test (C) and one-factor ANOVA with post hoc *t* test (A, B, E and F).

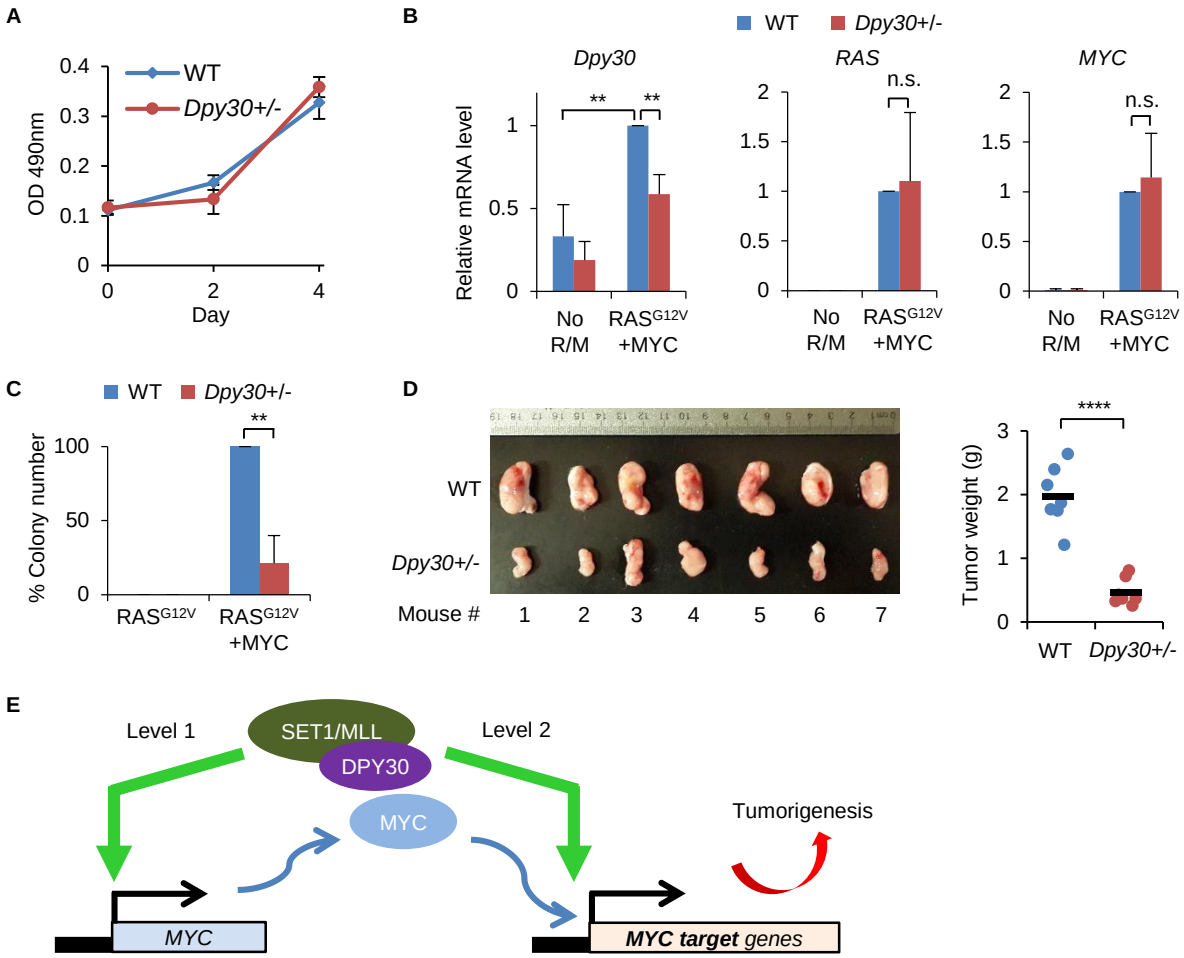

Figure 8. *Dpy30* is haploinsufficient for oncogenic transformation but not for cell growth. (A) WT and *Dpy30*$^{+/-}$ MEFs were assayed for growth, shown as the MTT assay results from three biological repeats. **(B and C)** Representative results of soft agar colony formation assay for HRAS^{G12V} and MYC-mediated oncogenic transformation of WT and *Dpy30*$^{+/-}$ MEFs. **(B)** Relative mRNA levels of *DPY30*, *RAS*, and *MYC* of untransduced MEFs and MEFs transduced with HRAS^{G12V} and MYC viruses were determined by qPCR and normalized to *Actb* from 3 independent transformation assays shown in (C) and (D). Levels in WT MEFs infected with HRAS^{G12V} and MYC were set to 1. **(C)** The percent colony numbers relative to WT (mean number was 59 for WT) were from 3 independent transformation assays using two different embryos-derived MEFs for each genotype. **(D)** WT and *Dpy30*$^{+/-}$ MEFs transduced with HRAS^{G12V} and MYC viruses were injected into the flanks of 7 NSG mice. Each mouse received WT MEFs on one flank and the *Dpy30*$^{+/-}$ MEFs on the other flank. Two weeks after injection, tumors were collected (in picture) and weighted. The tumor weights are plotted, where each dot represents a tumor from an animal. **(E)** A model illustrating the two different levels of regulation of MYC by DPY30 complexes. Data represent the mean ± SD (for A) or + SD (B and C). $^{**}P < 0.01$ and $^{****}P < 0.0001$ by one factor ANOVA with post hoc *t* test (B) and Student's *t*-test (C and D).

SUPPLEMENTAL INFORMATION

Hijacking a key chromatin modulator creates epigenetic vulnerability for MYC-driven cancer

Zhenhua Yang, Kushani Shah, Theodore Busby, Keith Giles, Alireza Khodadadi-Jamayran, Wei Li, and Hao Jiang

SUPPLEMENTAL METHODS

Flow cytometry analyses and sorting

Single cell suspensions were prepared from bone marrow, spleen or peripheral blood. Red blood cells were removed using ACK lysis buffer (0.15 M NH_4Cl, 10 mM $KHCO_3$, 0.1 nM EDTA, pH 7.2). For bone marrow and splenocyte analyses, cells were stained with antibodies for CD45R (RA3-6B2)-APC; IgM (RMM-1)-PE and IgD (11-26C.2A)-Pacific blue. FACS analysis was performed on LSRFortessa (Becton Dickinson), and data were analyzed using FlowJo software (Tree Star). B220+ spleen cells were enriched with magnetic CD45R (B220) microbeads (Miltenyi Biotec) following manufacturer's instructions. Proliferation and apoptosis were determined by BrdU incorporation and Annexin V staining assays, respectively, as previously described (1). Briefly, for BrdU analysis, 4-5 weeks old mice were intraperitoneally injected with 1.5mg BrdU at 6 hours prior to sacrifice. Cells were stained with cell surface antibodies as described above and then processed with BrdU staining using the FITC-BrdU Flow kit (BD Pharmingen) following the manufacturer's instructions. For apoptosis assays, cells were harvested and stained with antibodies as described above. After washing twice with cold PBS containing 3% heat-inactivated FBS, the cells were then incubated with FITC-Annexin V (BD Pharmingen) and 7-amino-actinomycin D (7-AAD) for 15 minutes in binding buffer (10mM HEPES, 140 mM NaCl and 2.5mM $CaCl_2$) at room temperature in dark. The stained cells were analyzed immediately by flow cytometry. Intracellular ROS levels were detected by ROS-ID™ Total ROS detection kit (Enzo Life Sciences, Cat# ENZ-51011) following manufacturer's instructions. Briefly, cells were stained with ROS detection reagent at 37°C for 15 min after being stained with the B220 antibody described as above. ROS levels in the gated population were quantified using flow cytometry. Proliferation and apoptosis assays for cultured P493-6 cells and transduced MEFs were performed similarly for the splenocytes, except that cells were incubated with BrdU for 30 min before the proliferation assays.

RNA extraction, chromatin immunoprecipitation (ChIP), ATAC assay, DNase I hypersensitivity assay, and quantitative PCR (qPCR)

Total RNAs were isolated using RNeasy Plus Mini Kit (Qiagen). Some of RNAs were reverse transcribed with SuperScript III (Invitrogen). ChIP assays were performed as described (2) using anti-Myc (Santa Cruz Biotechnology, sc-764x) and anti-H3K4me3 (Millipore 07-473). ATAC (3) and DNase I hypersensitivity (4) assays were performed following the published protocols with modifications. For ATAC assays, primary MEFs from *Dpy30*$^{F/F}$ and *CAG-CreER; Dpy30*$^{F/F}$ embryos (1) were treated with 4-hydroxytamoxifen at 0.5 μM for 4 days. 70,000 primary MEFs were used as input and for reaction with transposase. Cells were incubated with transposase for 45 minutes at 37°C with gentle agitation. Input samples were treated same as the transposase-incubated cells up until the transposase reaction step. Input samples were then sonicated for 45 minutes (instead of incubating with the transposase). qPCR was performed to detect change in accessibility upon *Dpy30* KO. Input was used to normalize transposase-treated samples. For DNase I hypersensitivity assays, 5 million spontaneously immortalized MEFs were used for each reaction. (The large number of cells required for DNase I hypersensitivity assay made it difficult to use primary early passage MEFs.) DNase I enzyme and reaction buffer were purchased from NEB (Cat# M0303L). Undigested and digested samples were

purified using PCR purification kit commercially available from Qiagen (Cat# 28106). qPCR was performed to detect change in accessibility upon Dpy30 KD. Undigested samples were used for normalization. qPCR was performed with SYBR Advantage qPCR Premix (Clontech) on a ViiA7 Real-Time PCR System (Applied Biosystems). Primers used are listed in Supplemental Table 7. Relative expression levels were normalized to *Actb*. For ChIP results, percent input was first calculated from ChIP qPCR results as described (2), and ChIP enrichment fold was calculated as the ratio of the percent input value for each locus over that for the indicated sites and samples.

Microarray, RNA-seq, ChIP-seq, and data analyses

For microarray analyses, total RNAs were labeled using the Illumina TotalPrep RNA Amplification Kit (Life Technologies, Cat# AMIL1791) following the manufacturer's protocol, and submitted to the Genomics Resource Center at the Rockefeller University for hybridization to the Illumina 12-sample BeadChip. Genes with Detection P value above 0.05 in all samples were filtered. Signals were normalized against the median in each sample.

For RNA-seq with spike-in control, the ERCC RNA Spike-In Mix (Ambion, 4456740) was used following instructions of the product. The amount of spike-in added was calibrated to the RNA yield to ensure the spike-in signal was in the appropriate dynamic range. Specifically, 2µl of a 1:200 diluted ERCC Spike-In Mix 1 was added to one of the samples that had a total RNA of 465ng. Between 1.8µl to 5.4µl of 1:200 diluted ERCC Spike-In Mix 1 were added to other samples (between 240 to 800ng total RNAs) at the same ratio of Spike-in/cell number.

Library preparation and sequencing for RNA and ChIP (and their corresponding input) DNA were performed at the Genomic Services Lab at HudsonAlpha Institute for Biotechnology (Huntsville, AL). Briefly, the quality of the total RNA and DNA was assessed using the Agilent 2100 Bioanalyzer. Two rounds of polyA+ selection was performed for RNA samples, followed by conversion to cDNAs. The mRNA library generation kits (Agilent, Santa Clara, CA) and TruSeq ChIP Sample Prep Kit (Illumina) were used generate sequencing libraries per manufacturer's instructions. The indexed DNA libraries were quantitated using qPCR in a Roche LightCycler 480 with the Kapa Biosystems kit for library quantitation (Kapa Biosystems, Woburn, MA) prior to cluster generation. Clusters were generated to yield approximately 725 K to 825 K clusters/mm2. Cluster density and quality were determined during the run after the first base addition parameters were assessed. Sequencing was performed on Illumina HiSeq2500 with sequencing reagents and flow cells providing up to 300 Gb per flow cell.

For RNA-seq, we obtained 35-55 million of 51bp paired end reads for each RNA sample. All the reads were mapped to the mouse reference genome (GRCm38/mm10) using TopHat (v2.0.13). The alignment was guided using a Gene Transfer File (GTF version GRCm38.85). Low quality mapped reads (MQ<30) were removed from the analysis. Read count tables were generated using HTSeq (v.0.6.0) based on the Ensembl gene annotation file (Ensembl GTF version GRCm38.85) (5). All the read count tables were then normalized based on their ERCC RNA Spike-In Mix size factors calculated using the DESeq R package (v.3.0), and Deferential Expression (DE) analyses were performed using DESeq (v3.0) (6). All of the downstream statistical analyses and generating plots were performed in R (v3.1.1) (http://www.r-project.org/). To generate the heat map, upregulated and downregulated genes were clustered separately using R dist function in Euclidian mode and then merged to maintain the clustered order of the genes. The values in the matrix were scaled based on columns and not rows using heatmap.2 R function to make the two different data comparable in a single heat map. KEGG pathway analysis was performed using clusterProfiler R package (v3.0.0) (7). Gene ontology analysis was performed with DAVID 6.7 (https://david-d.ncifcrf.gov/), GSEA was performed at http://software.broadinstitute.org/gsea/index.jsp. The gene sets were from GSE51011 (8). Myc bound genes were selected if the Myc ChIP signal was positive in either pre-tumor or tumor samples, and ranked by q value (pre-tumor vs. control) from lowest to highest. Myc-bound UP gene set contains the

top 500 genes that were upregulated with a q value less than 0.001, and Myc-bound DN gene set contains 891 genes that were downregulated with a q value less than 0.01, from control to pre-tumor samples. Genes were rank-ordered in descending order according to the fold change. The list of pre-ranked genes was analyzed with the gene set matrix composed file (.gmx) from curated data. Significant gene sets enriched by Dpy30 KD were identified using nominal P value of 0.05. All analyses were performed using GSEA v2.0 software with pre-ranked list and 1000 data permutations.

For ChIP-seq, we obtained 25-35 million of 50bp single end reads for each DNA sample. Fastq files were first quality filtered using the FASTX toolkit (http://hannonlab.cshl.edu/fastx_toolkit/index.html Key: citeulike:9103573) "fastq_quality_filter" tool, with the following arguments: -q 20 and –p 80, which outputs reads that have a mapq score of at least 20 at least 80% of the bases. The quality filtered reads were then collapsed to eliminate PCR duplicates using the FASTX toolkit "fastx_collapser". The resultant fasta file was aligned using STAR ver. 2.4 (9). The SAM file outputs were converted to BAM using samtools "view" (10) and the BAM converted to BED using BEDtools "bamToBed" (11). The coverage of H3K4me3 and Myc plus/minus 5kb of all transcription start sites (profiles) were generated using deepTools2.0 (12). The workflow was carried out as follows: BAM files were input into bamCoverage to generate a bigwig "bw" file using the –scale argument to normalize coverage according to reads per million. The bw file was then used as an input into the computeMatrix tool using the reference-point argument. The output file was then input into the plotProfile to generate the profiles. For each analysis the GENCODE hg19 genome was used with 52170 genes. Screen captures of coverage were generated from loading a tdf file into the integrative genomic viewer (IGV) (13). The tdf files were generated from bedgraph files using IGVtools "totdf". The bedgraph files were generated from BED files using the BEDTools "genomeCoverageBed" with the –bg option set and the "scale" set to reads per million. The correlations plots comparing Myc and H3K4me3 were done using bedTools coverageBed –counts to quantify the number of total reads that were present within 5kb of each transcription start site. The reads were then normalized to reads per million (RPM) and a scatterplot was generated in Rstudio. The R-squared and p-values of the correlation were generated using the Wilcox.test within Rstudio. Genes were sorted according to their overall MYC binding levels and binned into quintiles (first = top 20%, second = 21-40%, etc.). Box and Whisker plots were also generated in Rstudio using "boxplots".

Protein preparation, binding, and immunoblotting assays

MBP-tagged C-MYC was cloned into pMal-c2x (New England BioLabs, N8076S), and induced by Isopropyl β-D-1-thiogalactopyranoside (IPTG) in BL21 STAR DE3 *E. coli* cells (Invitrogen). Cells were lysed in 300mM KCl, 50mM Tris (pH 7.5), 20% Glycerol, 0.1% NP40, protease inhibitor cocktail (Roche), 0.5mg/ml lysozyme, sonicated and cleared by centrifugation. The supernatant was incubated with Amylose beads (NEB) at 4°C for 2 hours and extensively washed with BC500 (50 mM Tris [pH 7.4], 500 mM KCl, 20% glycerol, 0.2mM EDTA) and 0.5% NP40, followed by BC100 and 0.1% NP40. Bound protein was checked by SDS-PAGE and coomassie blue staining. To express ASH2L and DPY30, Sf9 insect cells (Invitrogen) were infected with baculoviruses expressing FLAG-ASH2L (F-ASH2L) and FLAG-HA-DPY30 (FH-DPY30)(2) for 72 hours. Cells were lysed in 500mM KCl, 50mM Tris (pH 7.5), 20% Glycerol, 0.1% NP40, protease inhibitor cocktail (Roche), and cleared by centrifugation. The supernatant was incubated with anti-FLAG M2 resin (Sigma) at 4°C for 6 hours and extensively washed with BC500 and 0.5% NP40, followed by BC100 and 0.1% NP40. Bound proteins were eluted with 0.4mg/ml FLAG peptide (Sigma) in BC100 and 0.1% NP40. For in vitro binding assays, 10μg MBP-MYC or 10 μg MBP on resin was pre-incubated with 200μl binding buffer (BC300, 0.05% NP40, and protease inhibitor cocktail), and further incubated at 4°C overnight after addition of 4 μg purified F-ASH2L or FH-DPY30. Resin was extensively washed with the binding buffer and was checked for bound proteins by SDS-PAGE and immunoblotting.

To determine protein expression levels, cells were lysed by lysis buffer (1% SDS, 10mM EDTA and 50mM Tris-Cl, pH 7.5) with fresh added Protease Inhibitor Cocktail (Roche) and boiled for 5 min. Proteins were resolved on SDS-PAGE gel followed by immunoblotting using antibodies described before (2) for Dpy30 and H3K4me3, from Santa Cruz Biotechnology for c-Myc (sc-764), β-Actin (sc-47778), and p53 (sc-6243), or from other commercial sources: anti-Gapdh (Chemicon, MAB374); anti-Flag (Sigma, A8592); anti-Flag (Sigma, A2220, M2 beads); anti-phospho-Histone H2A.X (Ser139) (Millipore, 05-636), and anti-MBP (New England BioLabs, E8032S). Key signals were quantified using ImageJ program followed by subtraction of a blank area and normalization to the indicated reference signal intensity.

SUPPLEMENTAL TABLE LEGENDS

Table S1. Microarray analyses of global gene expression in P493-6 cells.
P493-6 cells were stably infected with viruses expressing scramble control (Scr) shRNA, or two different shRNAs for *DPY30* (shRNA #2, D2 and shRNA #5, D5). Cells were subject to experimental scheme in Figure 2D. Microarray assays were performed using RNAs from cells treated with tetracycline for 3 days (to turn off Myc) and right before washing away tetracycline (0h) as well as from cells 4h after culture in Tetracycline-free medium after tetracycline withdrawal (4h).

Table S2. Genome-wide MYC binding in control and DPY30 KD P493-6 cells.
P493-6 cells were stably infected with viruses expressing scramble control (Scr) shRNA, or *DPY30* shRNA #2. MYC ChIP-seq results from these cells were analyzed. Genes were ranked in the order of the Control/KD ratio from highest to lowest.

Table S3. Genome-wide H3K4me3 in control and DPY30 KD P493-6 cells.
P493-6 cells were stably infected with viruses expressing scramble control (Scr) shRNA, or *DPY30* shRNA #2. H3K4me3 ChIP-seq results from these cells were analyzed.

Table S4. Curation of Myc targets for GSEA.
This file shows curation of genes from GSE51011 for use as gene sets in GSEA. Genes in the tab "Myc bound" are genes that have positive Myc ChIP signals in any of the P or T samples in the tab "All genes". Genes in the tab "Myc bound, up in EuMyc" are genes that that are upregulated from non-transgenic control to pre-tumor samples, and ranked from lowest (most significant) to highest (least significant) q value comparing pre-tumor and non-transgenic control. The top 500 genes were used in the "Myc bound UP" gene set for GSEA. Genes in the tab "Myc bound, down in EuMyc" are genes that that are downregulated from non-transgenic control to pre-tumor samples, and ranked from lowest (most significant) to highest (least significant) q value comparing pre-tumor and non-transgenic control. All genes with q value < 0.01 were used in the "Myc bound DN" gene set for GSEA.

Table S5. Clustered genes.
A total of 305 Genes that were down- or upregulated over 4 fold in the average of 4 *Eμ-Myc*; *Dpy30*$^{+/-}$ compared to *Eμ-Myc* animal-derived splenic B cells. Their Myc ChIP-seq signals at TSSs in pre-tumors of 3 *Eμ-Myc* animals from GSE51011 (samples GSM1234472, GSM1234473, and GSM1234474) are shown. The RNA-seq results of 4 different animals of each indicated genotype (with distinctive color labeling) were normalized to Spike-In RNA and shown after logarithmic transformation.

Table S6. Analyses of gene expression change by *Dpy30* heterozygosity.

The tab "down in at least 3 litters" shows genes that were downregulated over 1.2 fold in *Eμ-Myc; Dpy30*$^{+/-}$ compared to *Eμ-Myc* B cells in 3 out of the 4 sequenced litters (each litter has one mouse for each genotype). The tab "up in at least 3 litters" shows genes that were upregulated over 1.2 fold in *Eμ-Myc; Dpy30*$^{+/-}$ compared to *Eμ-Myc* B cells in 3 out of the 4 sequenced litters (each litter has one mouse for each genotype). The tab "KEGG and DAVID GO" shows the results of KEGG and DAVID GO analyses of genes in the other tabs.

Table S7. Primers used.

SUPPLEMENTAL REFERENCES

1. Yang Z, Shah K, Khodadadi-Jamayran A, and Jiang H. Dpy30 is critical for maintaining the identity and function of adult hematopoietic stem cells. *The Journal of experimental medicine.* 2016;213(11):2349-64.
2. Jiang H, Shukla A, Wang X, Chen WY, Bernstein BE, and Roeder RG. Role for Dpy-30 in ES Cell-Fate Specification by Regulation of H3K4 Methylation within Bivalent Domains. *Cell.* 2011;144(4):513-25.
3. Buenrostro JD, Wu B, Chang HY, and Greenleaf WJ. ATAC-seq: A Method for Assaying Chromatin Accessibility Genome-Wide. *Current protocols in molecular biology / edited by Frederick M Ausubel [et al].* 2015;109:21.9.1-9.
4. John S, Sabo PJ, Canfield TK, Lee K, Vong S, Weaver M, et al. Genome-scale mapping of DNase I hypersensitivity. *Current protocols in molecular biology / edited by Frederick M Ausubel [et al].* 2013;Chapter 27:Unit 21.7.
5. Anders S, Pyl PT, and Huber W. HTSeq--a Python framework to work with high-throughput sequencing data. *Bioinformatics (Oxford, England).* 2015;31(2):166-9.
6. Anders S, and Huber W. Differential expression analysis for sequence count data. *Genome biology.* 2010;11(10):R106.
7. Yu G, Wang LG, Han Y, and He QY. clusterProfiler: an R package for comparing biological themes among gene clusters. *Omics : a journal of integrative biology.* 2012;16(5):284-7.
8. Sabo A, Kress TR, Pelizzola M, de Pretis S, Gorski MM, Tesi A, et al. Selective transcriptional regulation by Myc in cellular growth control and lymphomagenesis. *Nature.* 2014;511(7510):488-92.
9. Dobin A, Davis CA, Schlesinger F, Drenkow J, Zaleski C, Jha S, et al. STAR: ultrafast universal RNA-seq aligner. *Bioinformatics (Oxford, England).* 2013;29(1):15-21.
10. Li H, Handsaker B, Wysoker A, Fennell T, Ruan J, Homer N, et al. The Sequence Alignment/Map format and SAMtools. *Bioinformatics.* 2009;25(16):2078-9.
11. Quinlan AR, and Hall IM. BEDTools: a flexible suite of utilities for comparing genomic features. *Bioinformatics (Oxford, England).* 2010;26(6):841-2.
12. Ramirez F, Ryan DP, Gruning B, Bhardwaj V, Kilpert F, Richter AS, et al. deepTools2: a next generation web server for deep-sequencing data analysis. *Nucleic acids research.* 2016;44(W1):W160-5.
13. Robinson JT, Thorvaldsdottir H, Winckler W, Guttman M, Lander ES, Getz G, et al. Integrative genomics viewer. *Nature biotechnology.* 2011;29(1):24-6.

Supplemental Figure 1

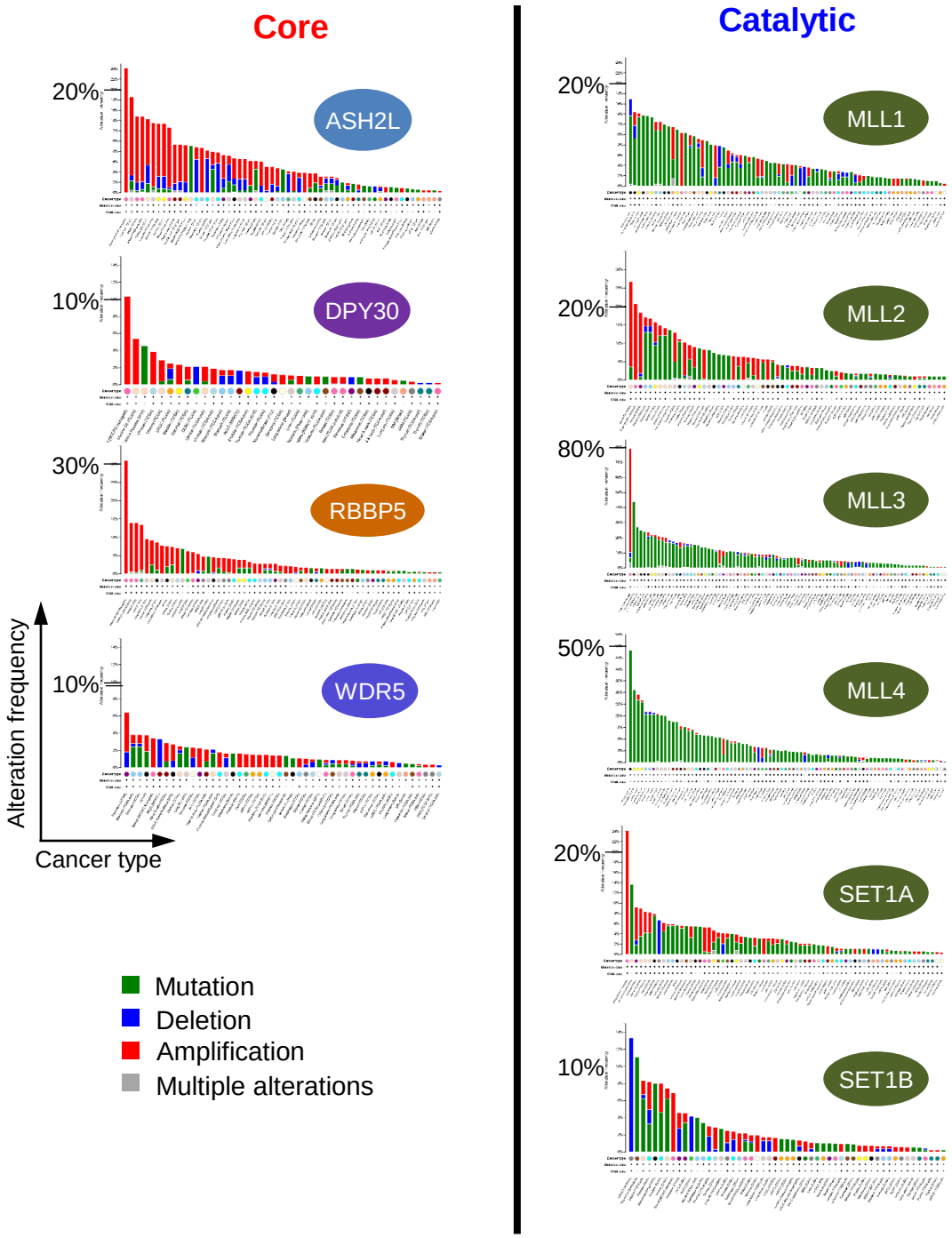

Supplemental Figure 1. Divergent alterations of the core versus catalytic subunits of the SET1/MLL complexes in human cancers.

Data were generated from cBioPortal (http://www.cbioportal.org/).

Supplemental Figure 2

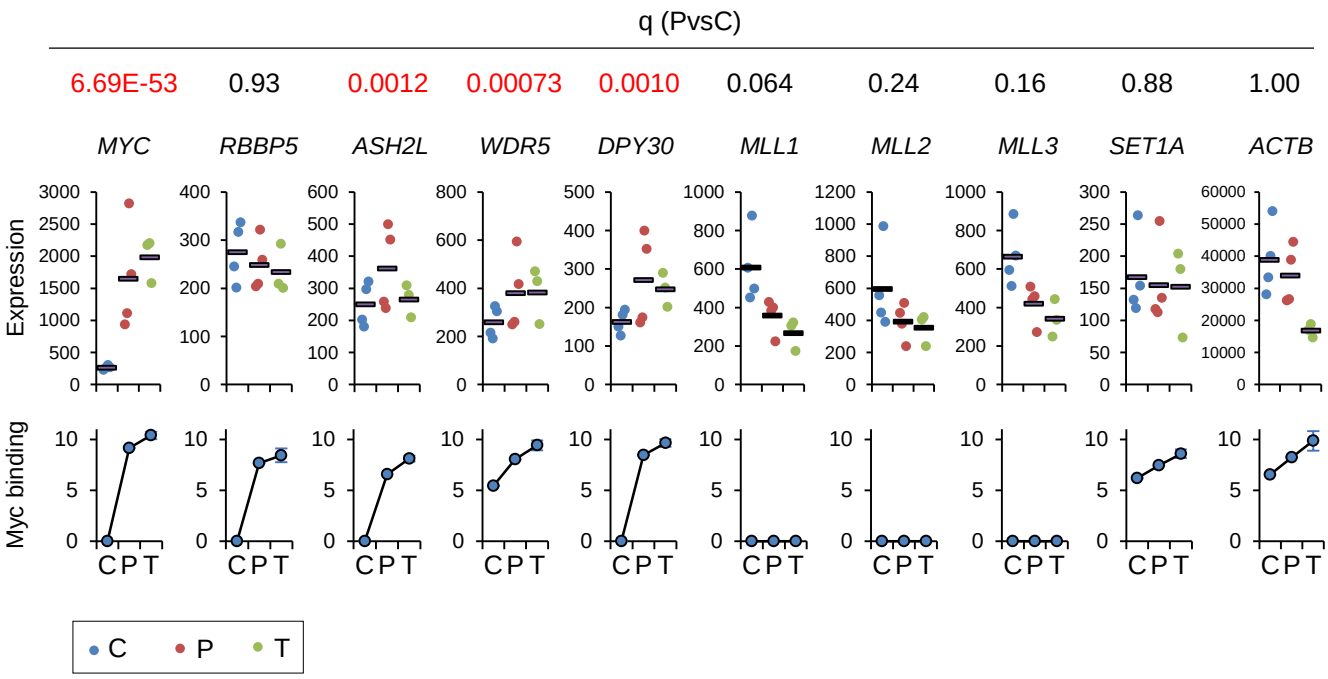

Supplemental Figure 2. MYC directly promotes the expression of the core subunits of SET1/MLL complexes.

Curated from GSE51011. Data on SET1B and MLL4 are not available. Top panels, expression levels of indicated genes from 4 control (C), 3 pre-tumor (P), and 3 tumor (T) samples normalized by mean expression level of all genes in each sample. False Discovery Rates (q value) between P vs. C are shown at the top, those < 0.05 in red. Bottom panels, MYC ChIP signal peak enrichment values at the promoters of indicated genes from one control, one pre-tumor, and 3 tumor samples shown as mean ± SD.

Supplemental Figure 3

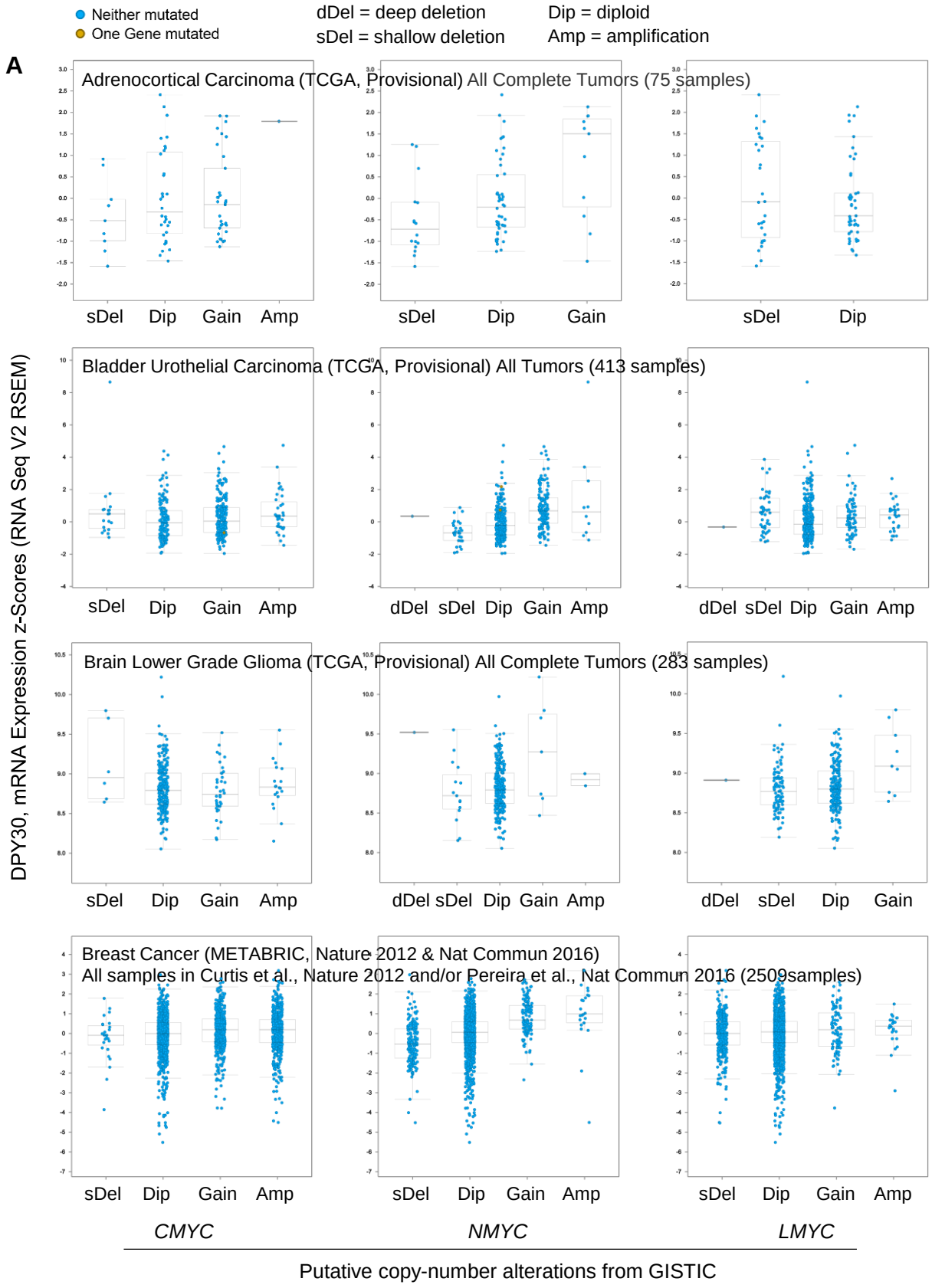

Supplemental Figure 3, continued 1

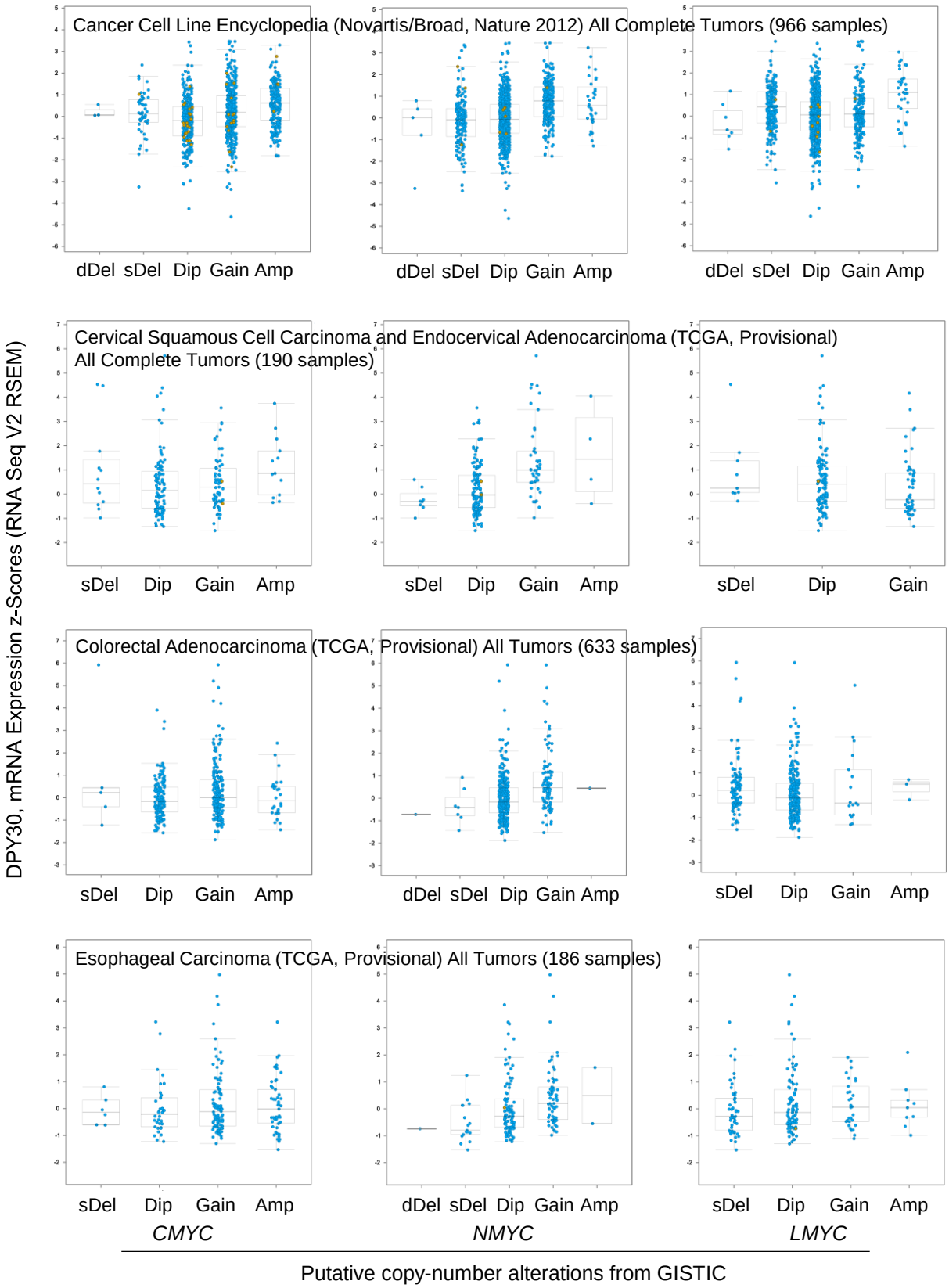

Supplemental Figure 3, continued 2

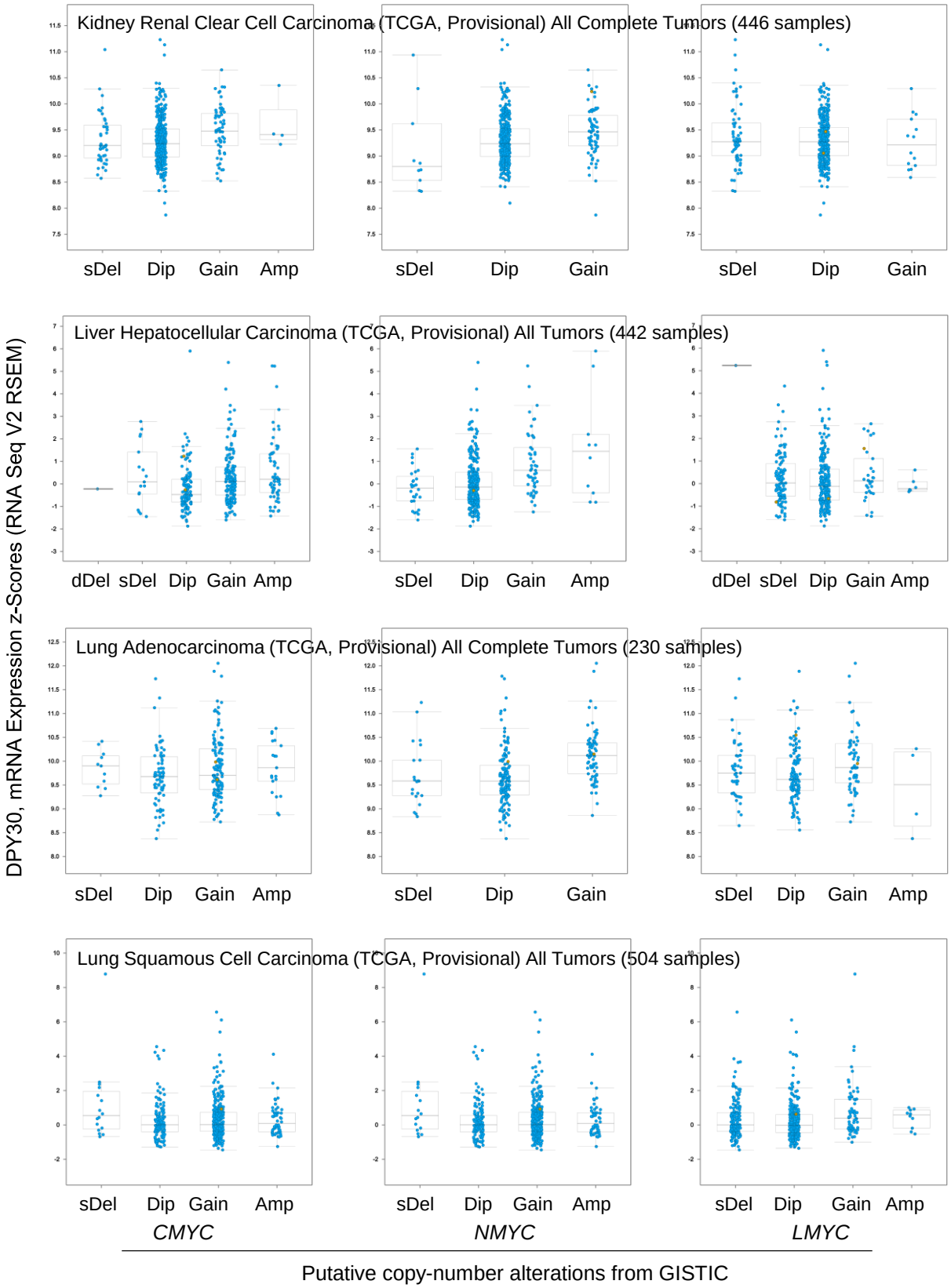

Supplemental Figure 3, continued 3

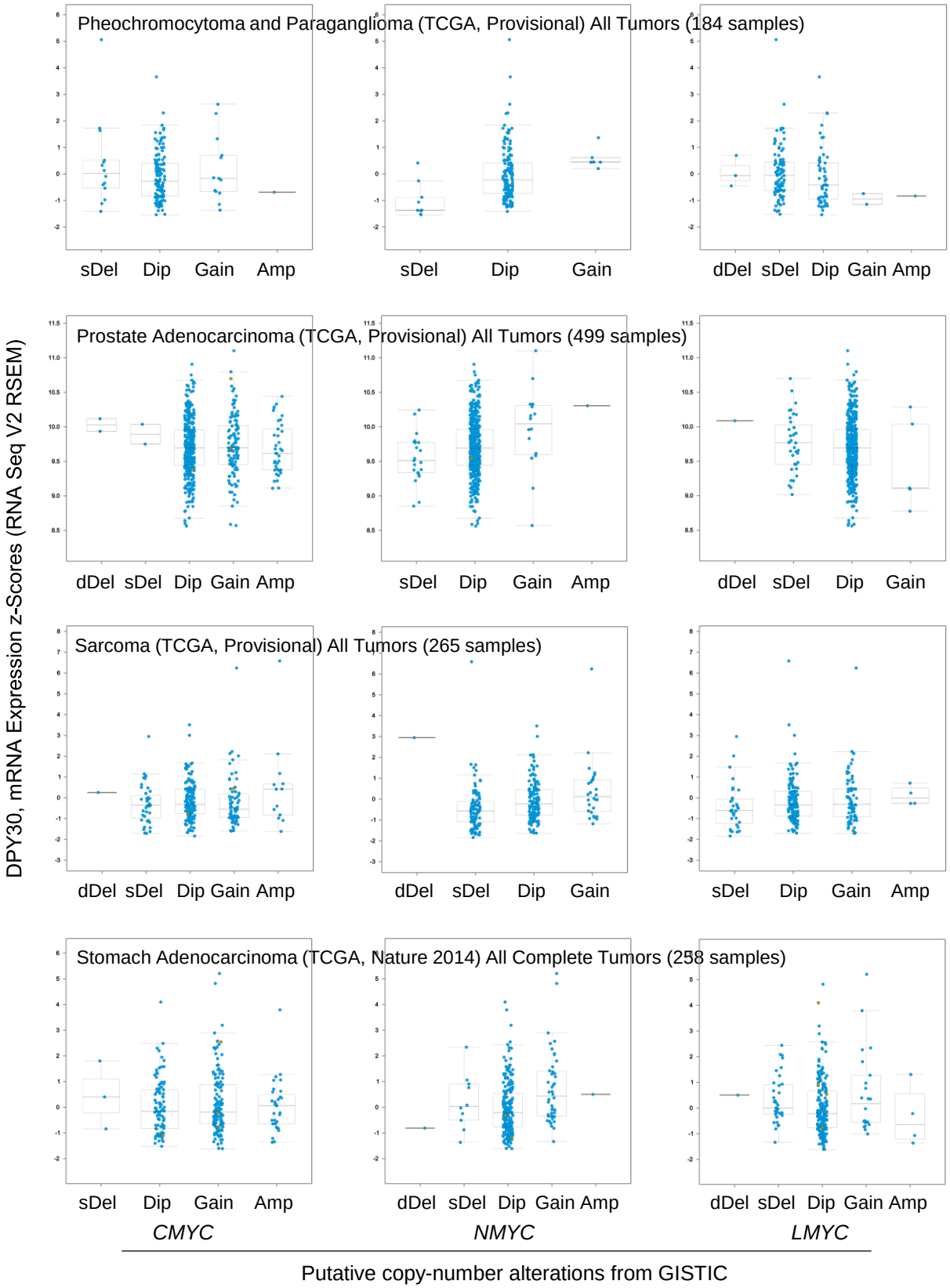

Supplemental Figure 3, continued 4

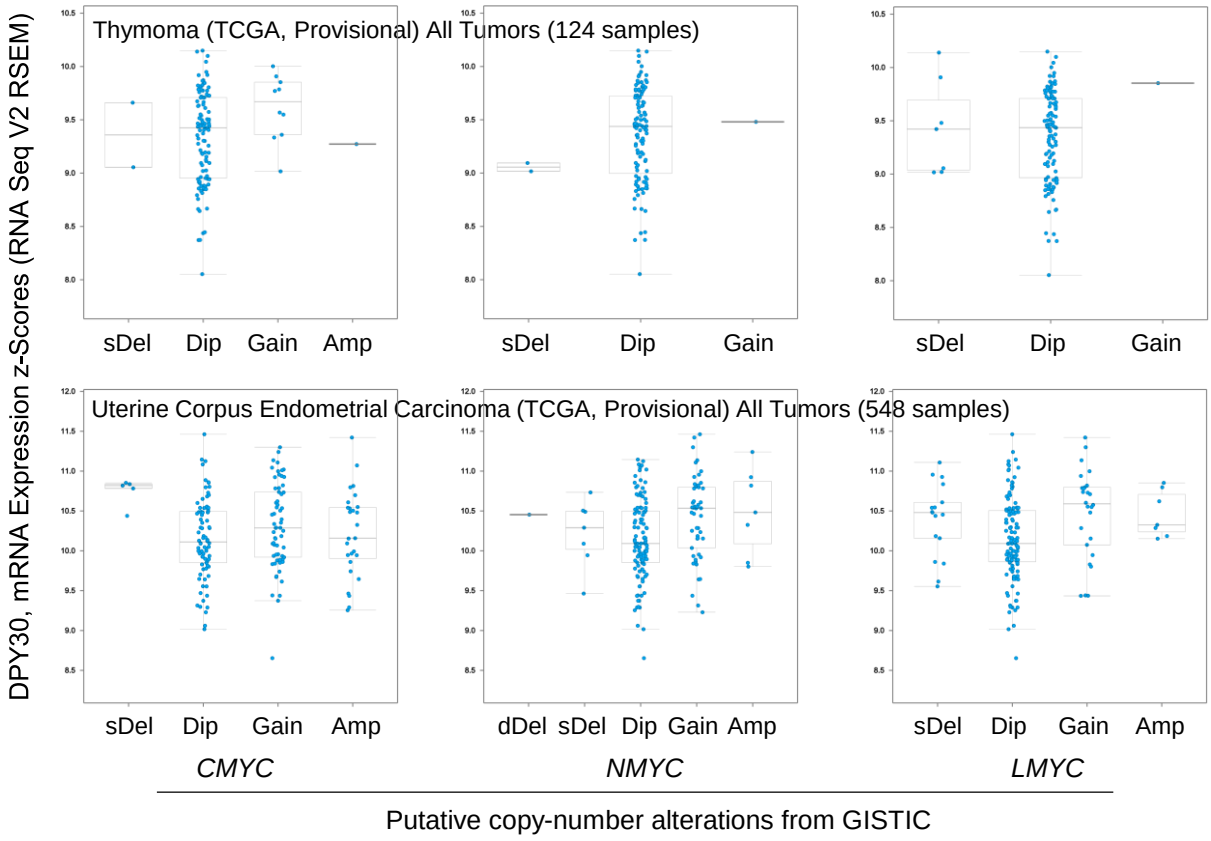

B

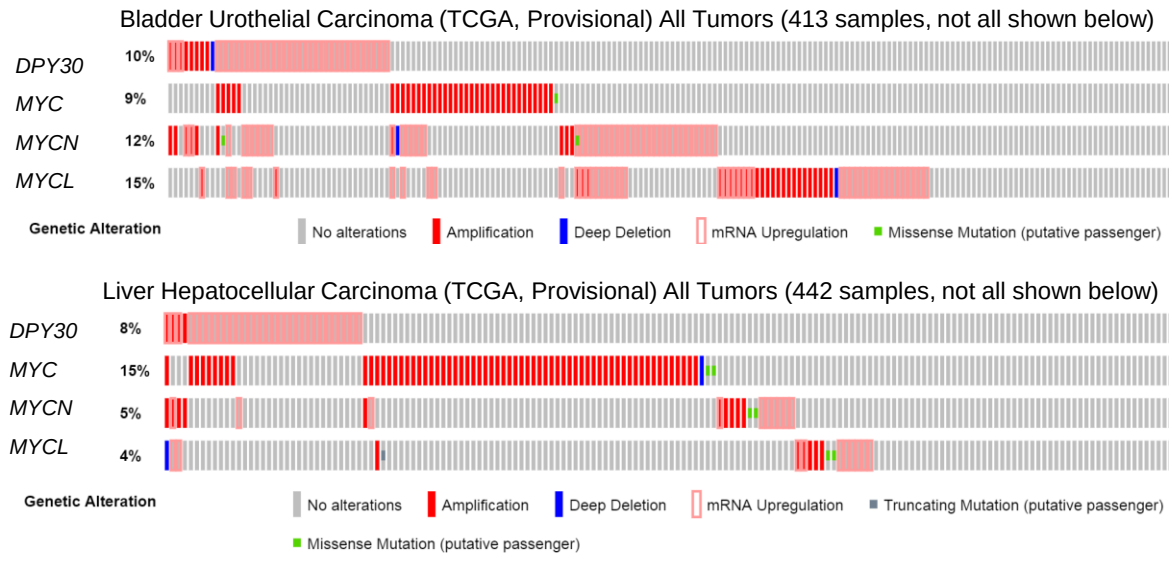

Supplemental Figure 3. Association of *MYC* gene amplification with *DPY30* expression in cancers.
(A) Plots of *DPY30* mRNA levels against copy-number alterations of *CMYC*, *NMYC*, and *LMYC* in a total of 18 cancer studies from cBioPortal that show notable elevation of *DPY30* expression with copy number increase (gain or Amplification) of one of more of the *MYC* genes. In all 169 studies in cBioPortal, 38 have over 50 samples and both copy number and mRNA expression results available. Note that increase of *Dpy30* level is associated with *CMYC* copy number increase in 7 studies, *NMYC* in 14, and *LMYC* in 3 studies.
(B) Oncoprint showing *DPY30* and *MYC* gene alterations in two different cancers. *MYC* = *CMYC*. Each small box represents a patient sample. All data in this figure are outputs from the cBioPortal.

Supplemental Figure 4

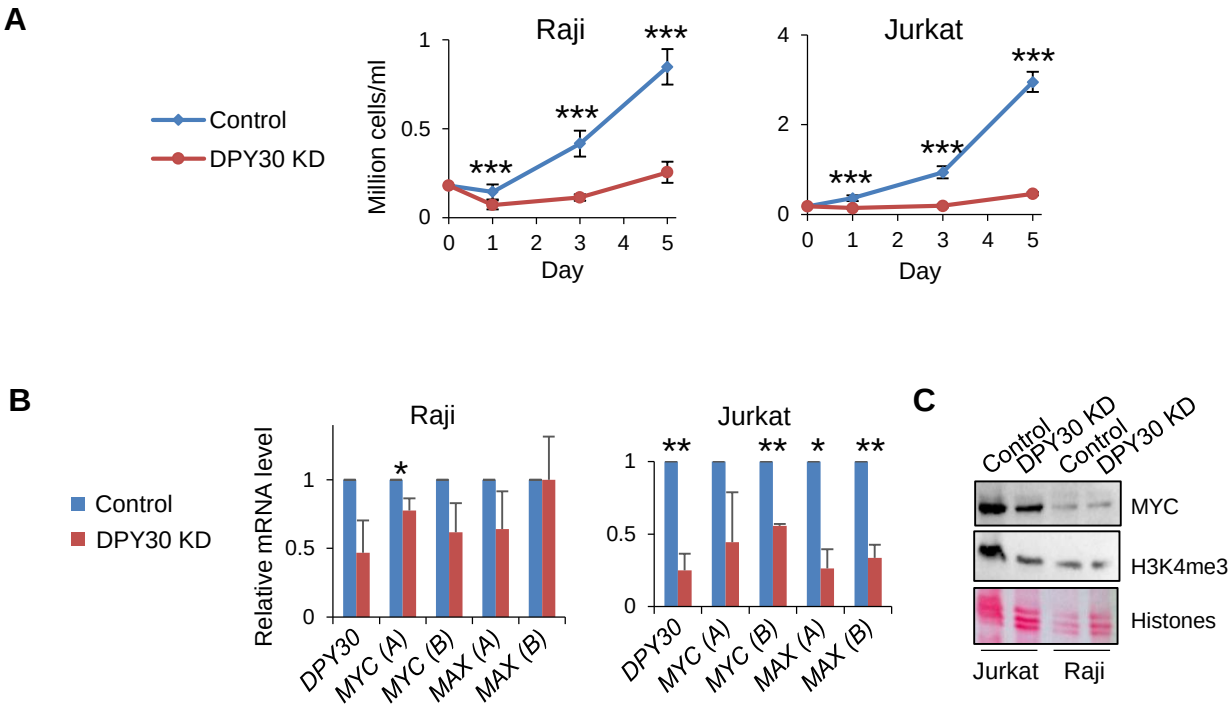

Supplemental Figure 4. DPY30 regulates expression of *MYC* in two blood cancer cell lines.

(A) Growth of Raji and Jurkat cells following DPY30 KD. Cell numbers were counted and mean ± SD from 3 independent KD assays are plotted.

(B) *DPY30*, *MYC,* and *MAX* mRNA levels were determined by qPCR using two different primers for *MYC* and *MAX* and normalized to *ACTB*, shown as mean + SD from 3 independent KD assays in Raji and Jurkat cells.

(C) Total cell lysates from control and DPY30 KD Raji and Jurkat cells were used for immunoblotting by indicated antibodies and for Ponceau S staining of histones.

Data represent the mean ± SD (A) or + SD (B). **P* < 0.05, ***P* < 0.01, and ****P* < 0.001 by Student's *t*-test.

Supplemental Figure 5

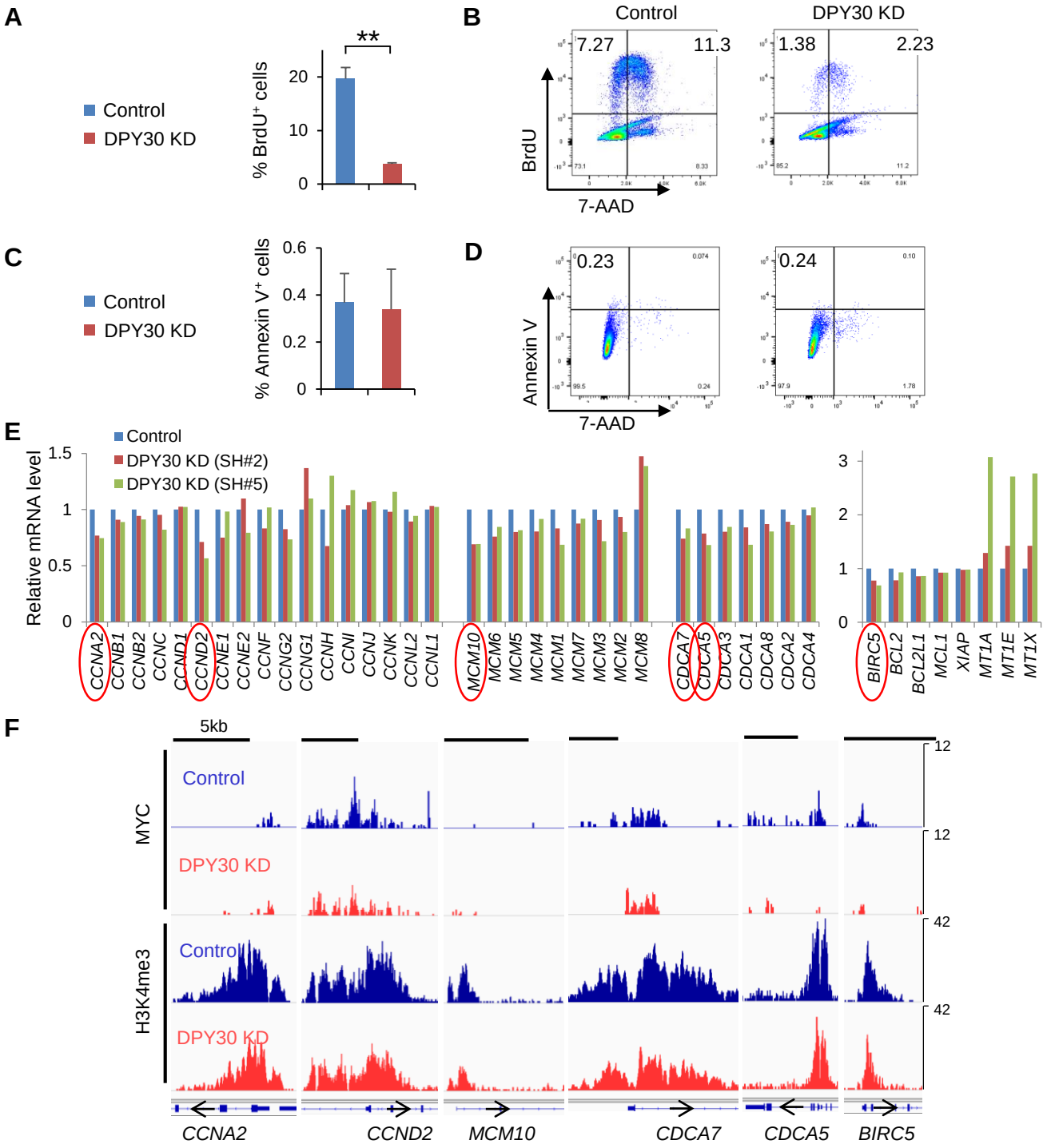

Supplemental Figure 5. Effects of DPY30 KD on proliferation and apoptosis of P493-6 cells.
All assays in this figure used control and DPY30 KD P493-6 cells. DPY30 KD was by DPY30 shRNA #2 except that both shRNA #2 and #5 were used in (E).
(A) BrdU$^+$ percentage in proliferation assays. A and C were from 5 repeats.
(B) Representative flow cytometry analysis results for proliferation assays.
(C) Annexin V$^+$ percentage in apoptosis assays.
(D) Representative flow cytometry analysis results for apoptosis assays.
(E) Relative mRNA levels of cell cycle regulator and pro-survival genes were analyzed by microarray assay. Genes in red circle were consistently downregulated by both DPY30 shRNAs.
(F) MYC binding and H3K4me3 profiles for circled genes in (E).
Data represent the mean + SD (A and C). $^{**}P < 0.01$ by Student's *t*-test.

Supplemental Figure 6

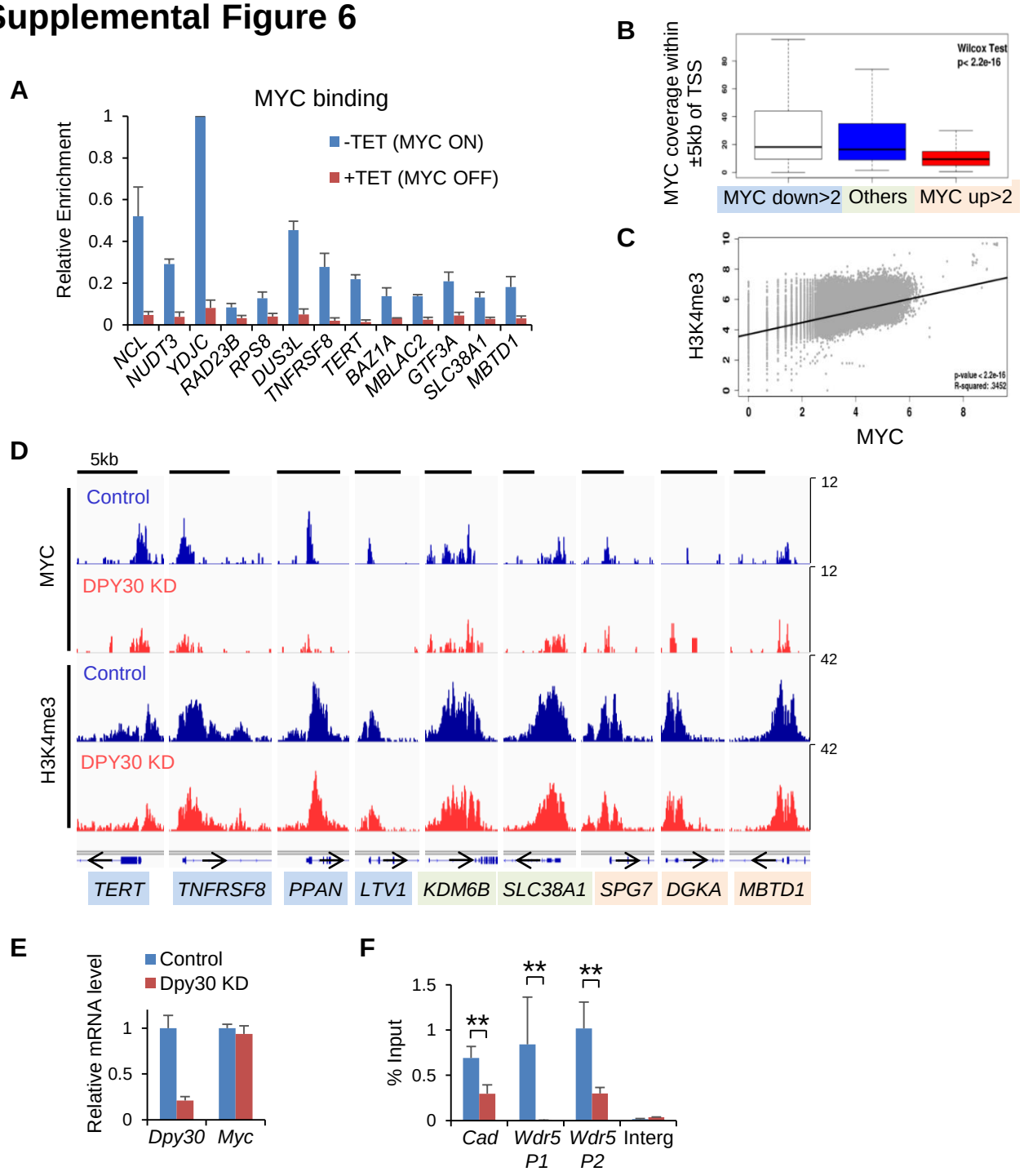

Supplemental Figure 6. DPY30 is important for efficient binding of MYC to its genomic targets.
(A) MYC ChIP-qPCR at indicated TSSs in P493-6 cells with or without tetracycline (Tet) treatment from 3 independent Tet treatments. Significant (P<0.01) for all genes.
(B) Box-and-Whisker plot of the MYC ChIP coverages in the control cells for the three groups of genes in Figure 3C. The box represents the 25th, 50th, and 75th percentiles of the data, and the whiskers represent the 5th and 95th percentiles. P value (=2.2e-16) for the last two gene groups was shown as calculated by Wilcoxon signed-rank test.
(C) Correlation of genome-wide MYC binding and H3K4me3, from ChIP results of control cells. R^2=0.3452.
(D) Representative MYC binding and H3K4me3 profiles for genes within each group shown in Figure 3C.
(E) Relative mRNA levels of Dpy30 and Myc in MEFs expressing scramble (control) or Dpy30 shRNA (KD), normalized to *Actb* from triplicate measurements.
(F) Myc ChIP results of at indicated loci from triplicate measurements in MEFs in (E).
Data represent the mean + SD (A, E, and F). ***P* < 0.01 by Student's *t*-test.

Supplemental Figure 7

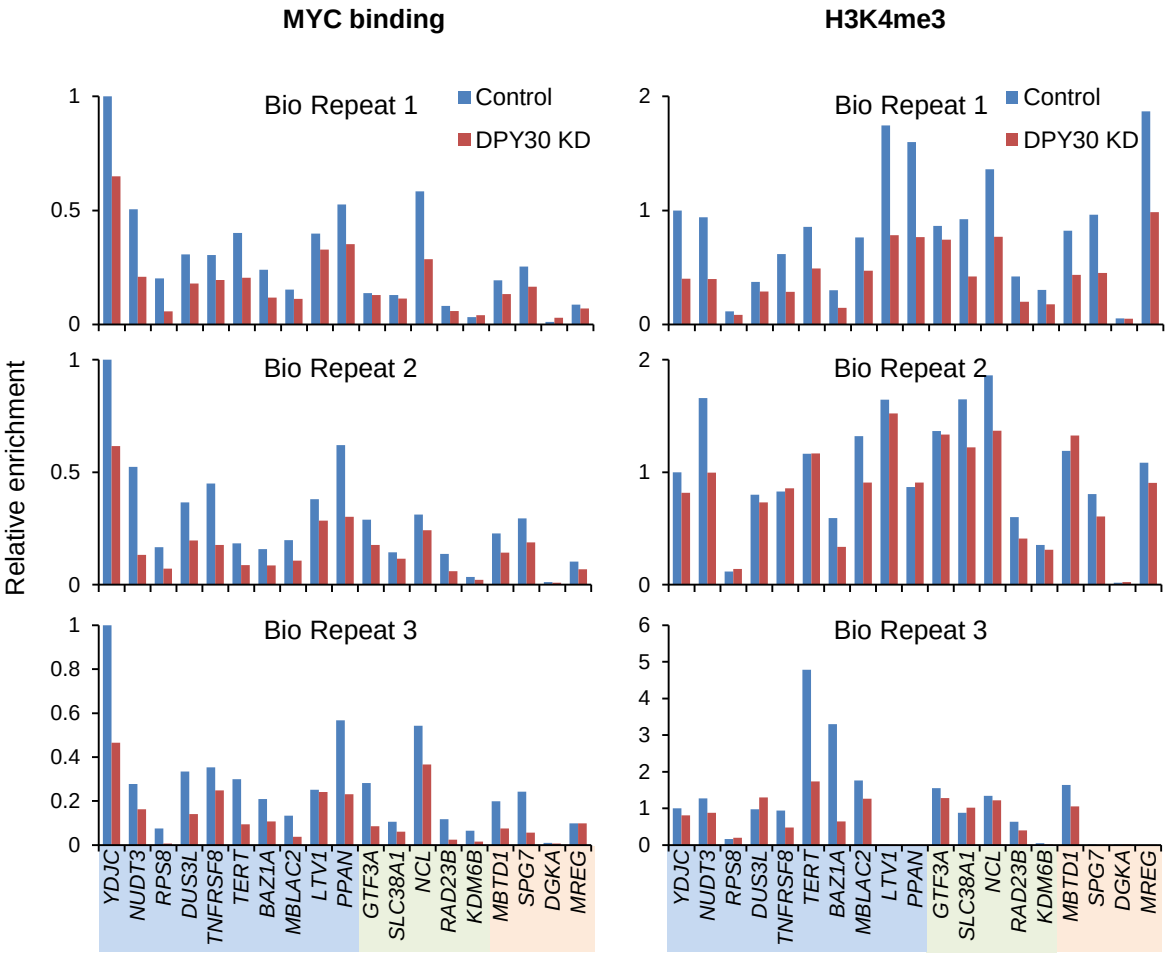

Supplemental Figure 7. Effects of DPY30 KD on MYC binding and H3K4me3 at selected genes in P493-6 cells.

MYC and H3K4me3 ChIP at TSSs by qPCR, calculated from the ratio of the percent input value for each locus over that for the *YDJC* site in the control sample in 3 individual biological repeats. Each repeat is an independent KD followed by ChIP assay in P493-6 cells.

Supplemental Figure 8

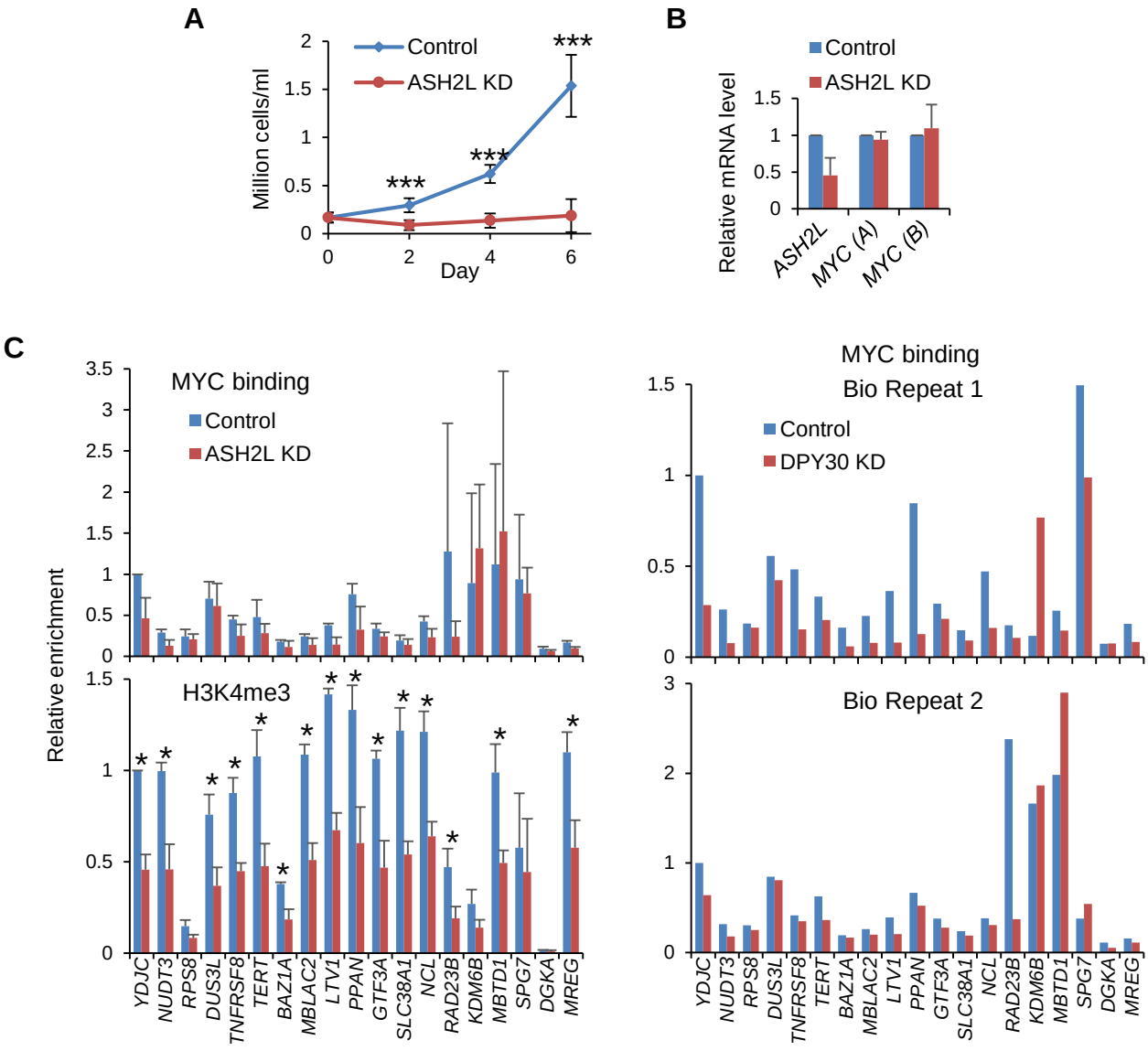

Supplemental Figure 8. Effects of ASH2L KD on P493-6 cells.

(A) Growth of P493-6 cells following ASH2L KD. Cell numbers counted from 4 independent KD assays are plotted.

(B) *ASH2L*, *MYC,* and *MAX* mRNA levels were determined by qPCR using two different primers for *MYC* and *MAX* and normalized to *GAPDH* from 4 independent KD assays.

(C) The same genes shown for DPY30 KD in Figure 3E were validated for MYC and H3K4me3 ChIP at TSSs by qPCR, calculated from the ratio of the percent input value for each locus over that for the *YDJC* site in the control sample. Shown on the left are from 2 (MYC) or 3 (H3K4me3) independent KD and ChIP assays in P493-6 cells, and shown on the right are the individual 2 independent KD and MYC-ChIP assays.

Data represent the mean ± SD (A) or + SD (B and C). **P* < 0.05, and ****P* < 0.001 by Student's *t*-test.

Supplemental Figure 9

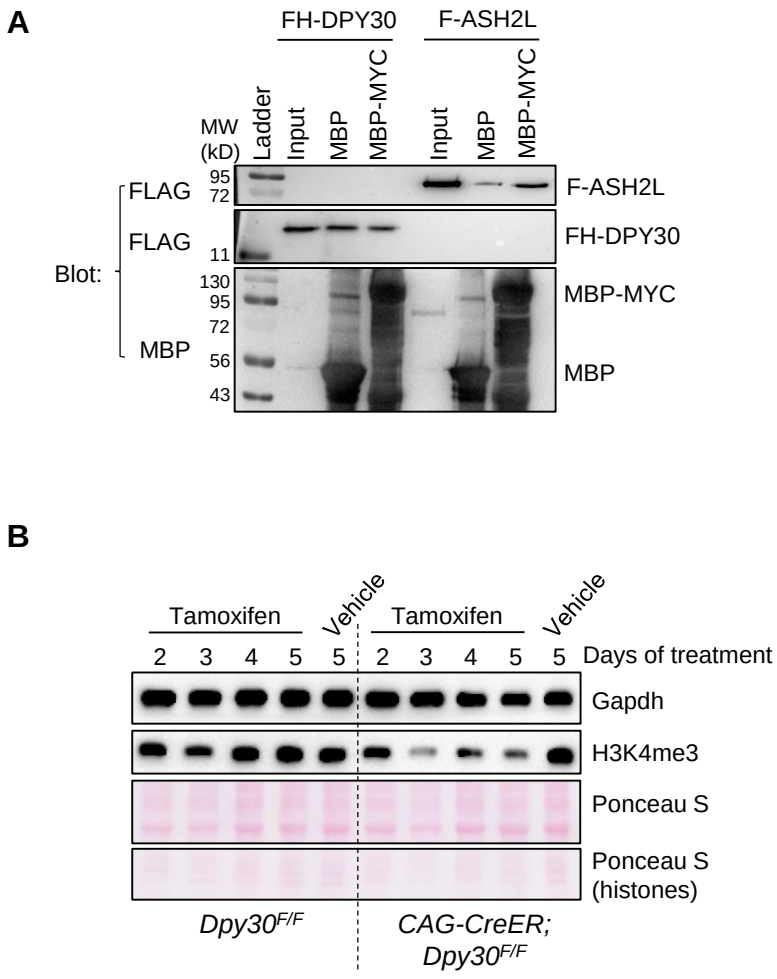

Supplemental Figure 9. On mechanisms by which DPY30 regulates genomic binding of MYC.
(A) Binding assay using all purified proteins. MBP or MBP-MYC protein immobilized on amylose resins were incubated with FLAG-HA-tagged DPY30 or FLAG-tagged ASH2L proteins followed by immunoblotting. Specific binding of ASH2L or DPY30 with MYC is shown by the relative FLAG tag signals bound to MBP-MYC versus MBP.
(B) Primary MEFs derived from *Dpy30$^{F/F}$* (control) or *CAG-CreER; Dpy30$^{F/F}$* (KO) mice were treated with 4-hydroxytamoxifen or vehicle (ethanol) for indicated days followed by immunoblotting.

Supplemental Figure 10

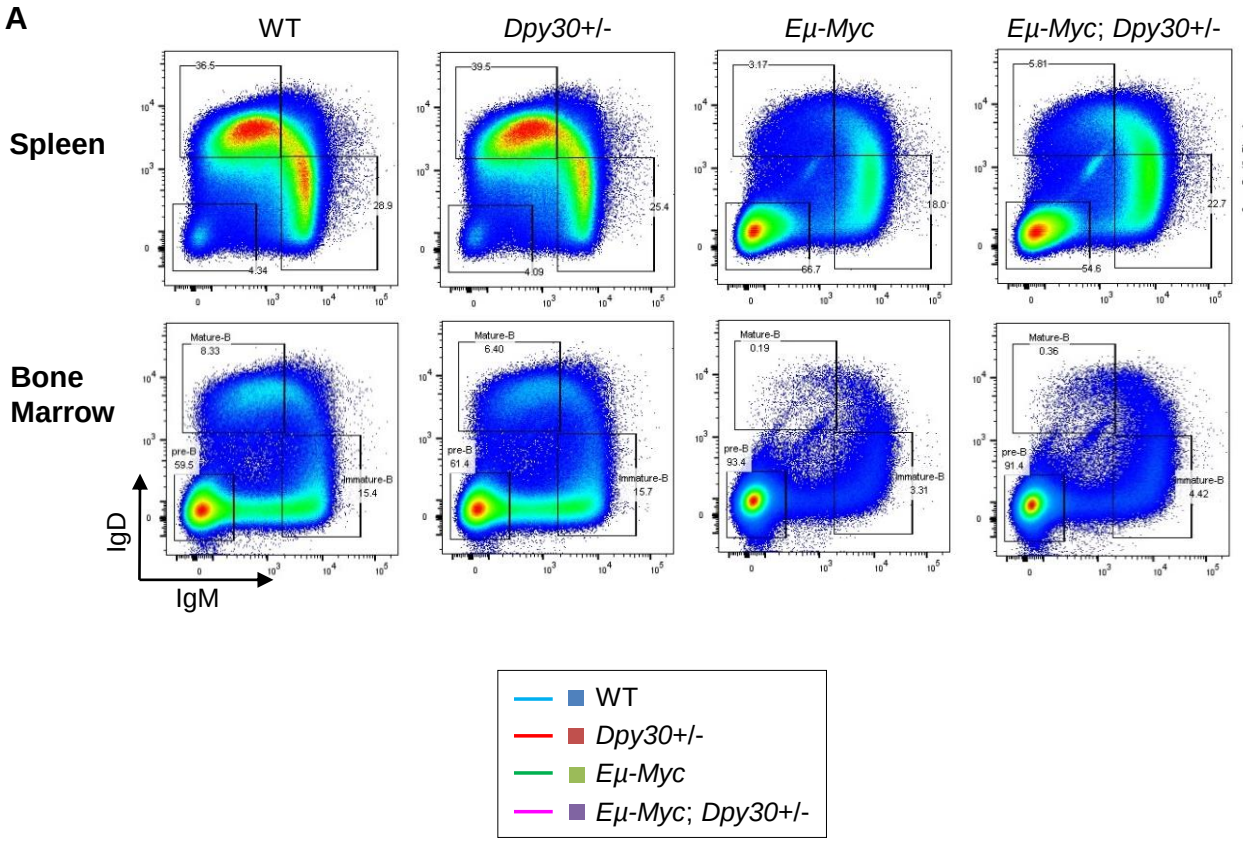

Supplemental Figure 10. Effects of *Dpy30* heterozygosity on B cell development and cellular damage response, with or without Myc hyperactivation.

(A) Representative FACS analysis of cell surface IgD and IgM in B220^{+} bone marrow and spleen cells of indicated genotypes.

(B) Immunoblotting for indicated proteins in B220^{+} cells from individual mice of indicated genotypes from two different litters.

(C) Intracellular ROS levels were determined for B220^{+} cells from different genotypes. A representative FACS analysis from one litter is shown on left, and results from multiple littermates are plotted on right as mean + SD. WT, n = 2; *Dpy30*$^{+/-}$, n = 2; *Eμ-Myc*, n = 4; and *Eμ-Myc; Dpy30*$^{+/-}$, n = 3.

Supplemental Figure 11

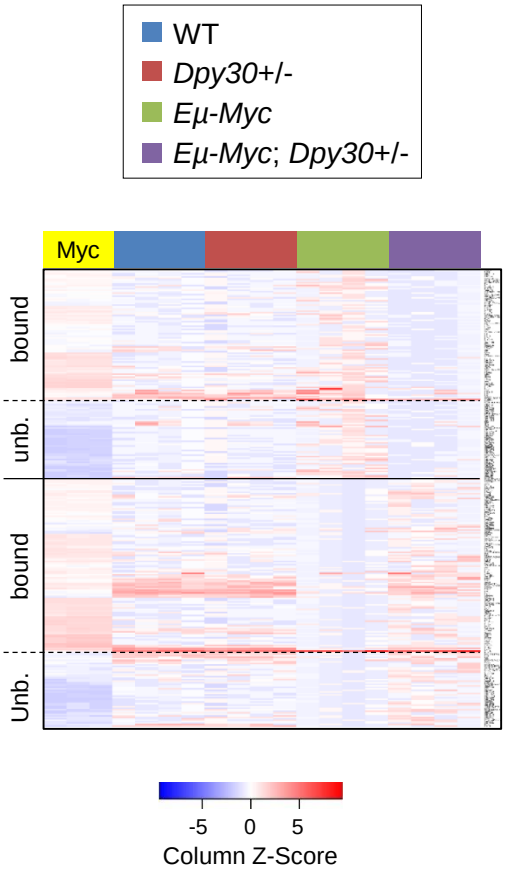

Supplemental Figure 11. Impact of *Dpy30* heterozygosity on gene expression in splenic B cells.

Heatmap showing relative expression levels of 305 genes that were down- or up-regulated (divided by the solid horizontal line) over 4 fold in the average of 4 (in each column) *Eμ-Myc*; *Dpy30*$^{+/-}$ compared to *Eμ-Myc* animal-derived splenic B cells. Genes are further clustered into Myc-bound and unbound (divided by the dash lines) based on Myc ChIP-seq signals (Myc, highlighted in yellow) at TSSs in pre-tumors of 3 *Eμ-Myc* animals from GSE51011 (samples GSM1234472, GSM1234473, and GSM1234474). The RNA-seq results of 4 different animals of each indicated genotype were normalized to Spike-In RNA and reflect per cell expression. More information of the clustered genes is in Supplemental Table 5.

Supplemental Figure 12

A

Enrichment of genes **downregulated** in *Eμ-Myc; Dpy30+/-* B cells:

KEGG Pathway Term	q value	Gene
Ribosome biogenesis in eukaryotes	0.0022	Nhp2l1/Gnl3/Nxf1/Nxt1/Nop10/Nop56/Nob1/Mphosph10/Fcf1/Rpp25/Taf9/Wdr3
Spliceosome	0.02	Srsf10/Hspa2/Srsf3/Snrpd1/Nhp2l1/Sf3b6/Magohb/Ncbp2/Ppil1/Prpf3/Snrpd2/Srsf7
RNA transport	0.026	Eif1a/Eif2s1/Eif4e/Sap18/Smn1/Tacc3/Nxf1/Nxt1/Magohb/Ncbp2/Eif3j1/Rpp25/Nup54

Enrichment of genes **upregulated** in *Eμ-Myc; Dpy30+/-* B cells:

KEGG Pathway Term	q value	Gene
Cytokine-cytokine receptor interaction	4.78E-14	Ccr6/Ccr1/Ccr9/Ccr2/Ccr5/Ccr10/Ackr3/Csf2rb/Csf2rb2/Csf3r/Cx3cr1/Egf/Egfr/Fasl/Flt1/Cxcl10/Il18rap/Il18r1/Il2rb/Il9r/Kdr/Ltb/Pdgfa/Ccl5/Tgfb3/Tnf/Tnfrsf17/Tnfrsf18/Cd27/Xcr1/Ifnlr1
Hematopoietic cell lineage	1.58E-11	Cd3d/Cd3e/Cd3g/Cd4/Cd5/Cd7/Cd8a/Cd8b1/Cd9/Cr2/Csf3r/Fcer2a/Il9r/Itga2/Itgb3/Anpep/Tnf
Natural killer cell mediated cytotoxicity	6.13E-08	Cd247/Fasl/Gzmb/Klra3/Klra4/Klra7/Klra8/Klrc1/Klrd1/Klrb1c/Ncr1/Nfatc2/Prf1/Tnf/Hcst/Klrk1
Antigen processing and presentation	8.91E-05	Cd4/Cd8a/Cd8b1/H2-Q7/H2-Q8/Klrc1/Klrd1/Tnf/H2-Q6

B

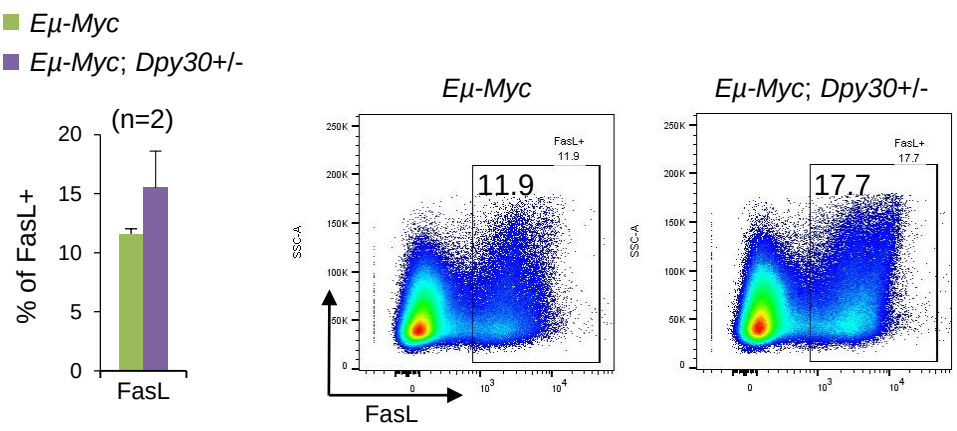

Supplemental Figure 12. *Dpy30* heterozygosity suppresses Myc-driven lymphomagenesis.
(A) KEGG analyses for genes that were down- or up-regulated over 1.2 fold in at least 3 out of 4 *Eμ-Myc; Dpy30*$^{+/-}$ compared to littermate *Eμ-Myc* splenic B cell samples, based on the RNA-seq results. The complete results of KEGG analyses are in Supplemental Table 6.
(B) FACS analysis of cell surface expression of FasL from 2 animals of each indicated genotype as mean + data range. Representative plots are shown on the right.

Supplemental Figure 13

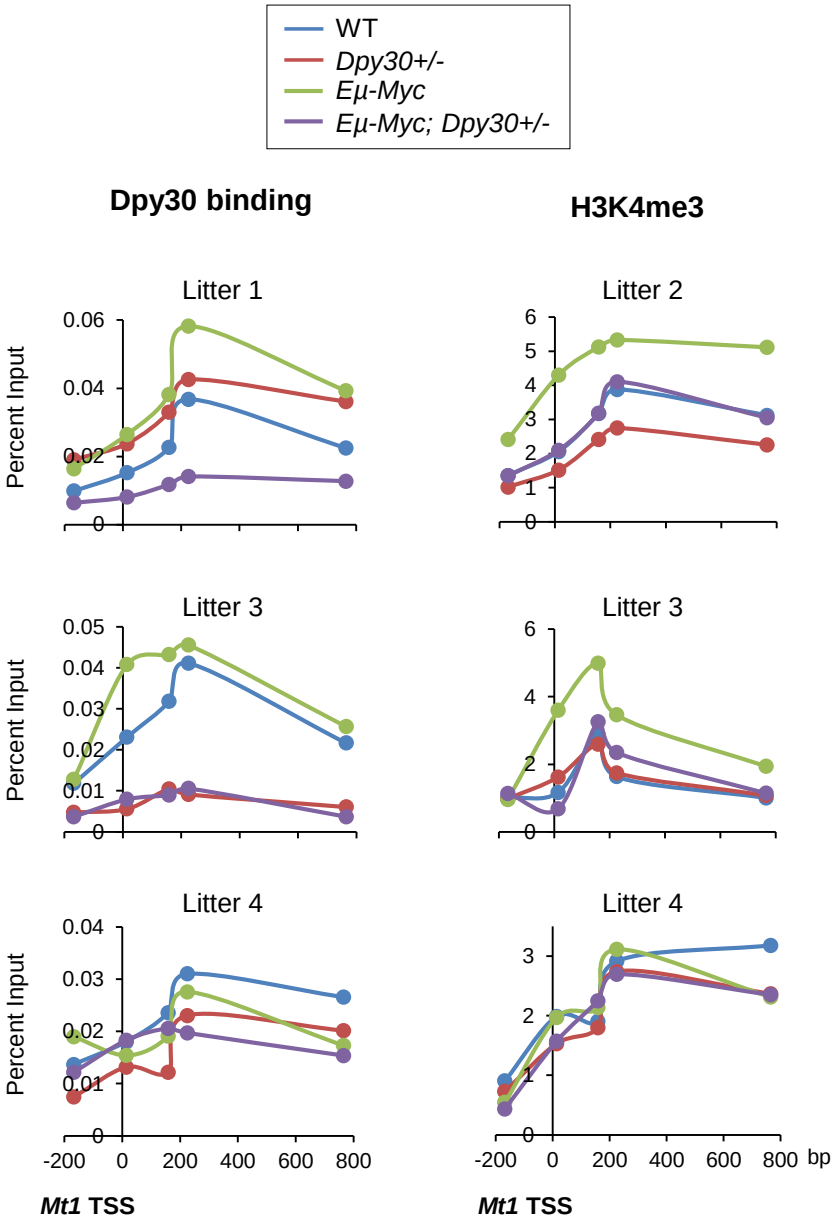

Supplemental Figure 13. Effects of *Dpy30* heterozygosity on Dpy30 binding and H3K4me3 at *Mt1*.

Dpy30 and H3K4me3 ChIP assays were performed using splenic B220+ cells from littermate mice of different genotypes, followed by qPCR using a series of primers around *Mt1* gene TSS. Each dot represents a primer pair with their relative distance to *Mt1* TSS shown on x-axis.

Supplemental Figure 14

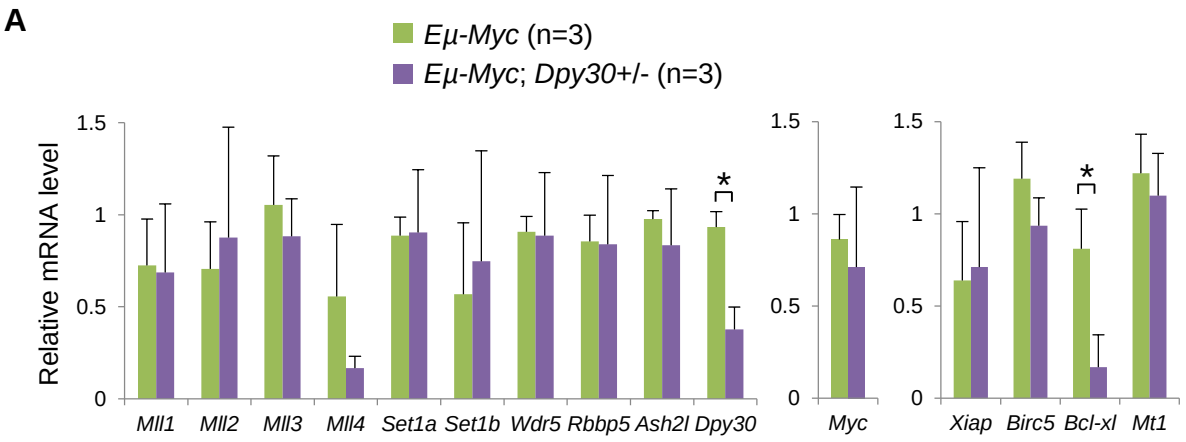

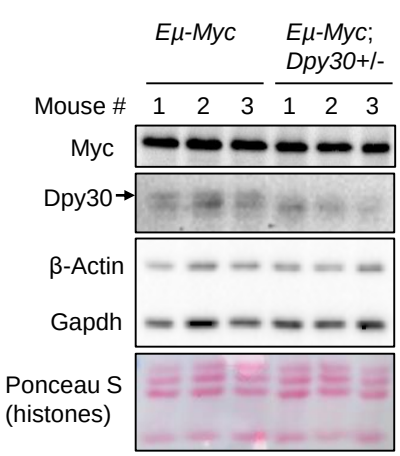

Supplemental Figure 14. Effects of *Dpy30* heterozygosity on gene expression in tumors that eventually form.

(A) Relative mRNA levels of genes encoding subunits of Set1/Mll complexes, *Myc*, and pro-survival genes from tumors that eventually formed in 3 *Eμ-Myc* mice and 3 *Eμ-Myc; Dpy30*$^{+/-}$ mice were determined by qPCR and normalized to *Actb*, shown as mean + SD. **P* < 0.05 by Student's *t*-test.

(B) Levels of indicated proteins in tumors that eventually formed in 3 *Eμ-Myc* mice and 3 *Eμ-Myc; Dpy30*$^{+/-}$ mice were determined by immunoblotting following resolution on SDS-PAGE gel. Note for the Dpy30 blot, the top band is specific for Dpy30 while the bottom band is a non-specific signal.

Supplemental Figure 15

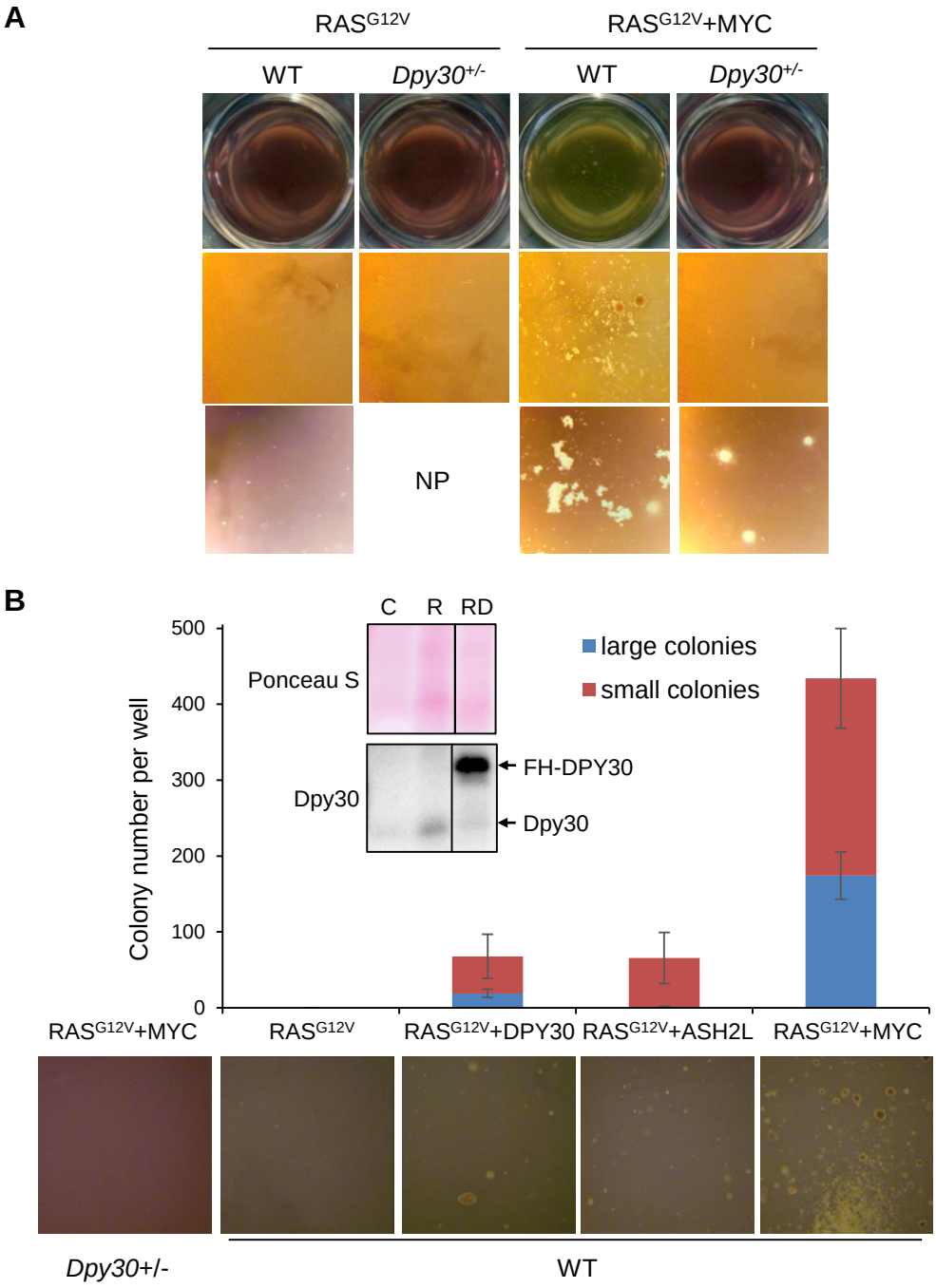

Supplemental Figure 15. Effects of *Dpy30* expression on cellular transformation.

(A) Representative image of wells and colonies from soft agar colony formation assay for $HRAS^{G12V}$ and MYC-mediated oncogenic transformation of WT and *Dpy30*$^{+/-}$ MEFs. NP, no pictures were taken.

(B) WT and *Dpy30*$^{+/-}$ MEFs (indicated at bottom) were transduced with combination of viruses as indicated (above images) and subjected to colony formation assay in soft agar. Colony numbers were plotted as mean ± SD from 6 independently seeded wells in one colony formation assays representative of two independent transduction assays, which showed consistent phenotype. large colonies are those larger than 0.2 mm in diameter. This was arbitrarily set as the cutoff. $P < 0.00001$ for the large colonies between $HRAS^{G12V}$+DPY30 (we used FLAG-HA-tagged DPY30 or FH-DPY30) and $HRAS^{G12V}$+ASH2L. Inserts: Ponceaus S staining and anti-Dpy30 immunoblotting for total lysates of WT MEFs untransduced (C) or transduced with $HRAS^{G12V}$ (R) or with $HRAS^{G12V}$+FH-DPY30 (RD). Overall effect on the colony numbers was analyzed separately for large and small colonies, using one-factor ANOVA with post hoc *t* test.

Supplemental Figure 16

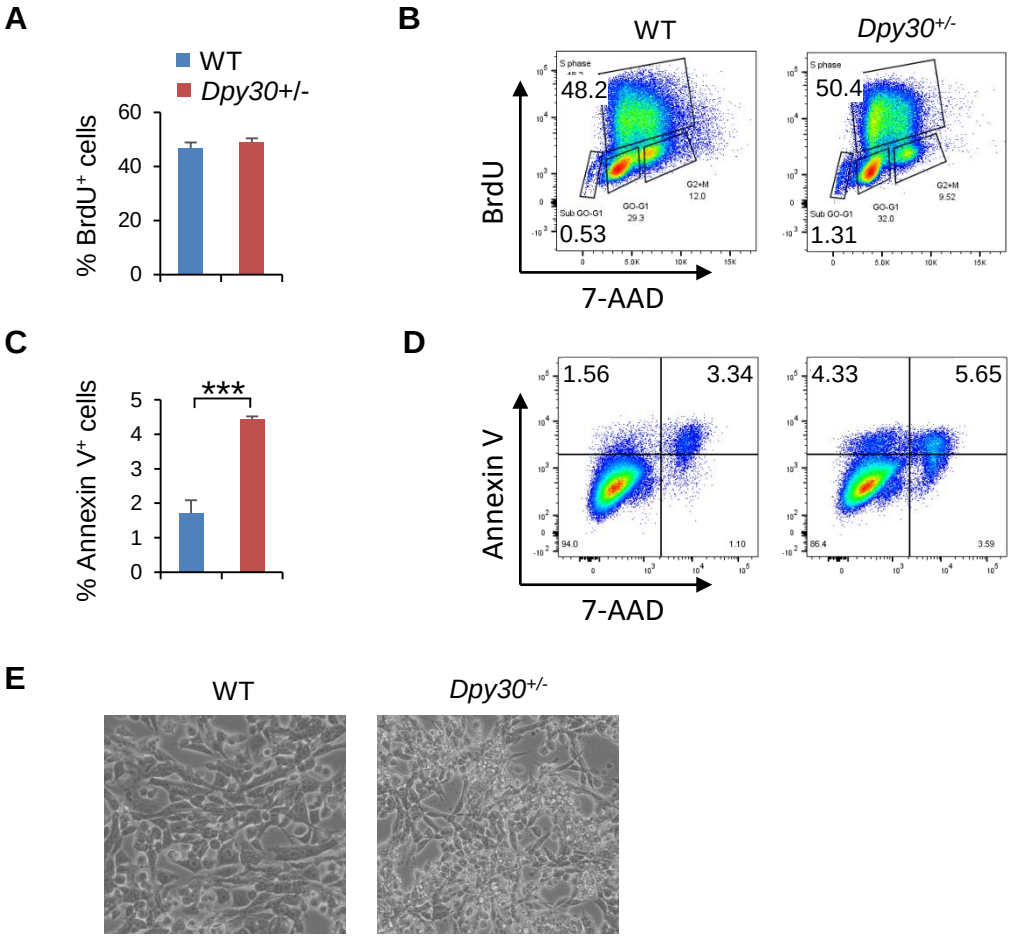

Supplemental Figure 16. **Effects *Dpy30* heterozygosity and proliferation and death of MEFs.** All assays in this figure used WT and *Dpy30*$^{+/-}$ MEFs after transduction with HRAS^{v12} and MYC.

(A) BrdU^{+} percentage in proliferation assays. In A and C, Average ± SD from six repeats are plotted. *** P<0.001 by Student's t-test.

(B) Representative flow cytometry analysis results for proliferation assays.

(C) Annexin V^{+} percentage in apoptosis assays.

(D) Representative flow cytometry analysis results for apoptosis assays.

(E) Representative images of the cells in culture. Note the large number of detached and round-up *Dpy30*$^{+/-}$ MEFs after transduction with HRAS^{v12} and MYC.